Electron trajectories in a helical free-electron laser with an axial guide field

J. T. Donohue and J. L. Rullier*
Laboratoire de Physique Théorique, Université de Bordeaux I, 33170 Gradignan, France
(Received 2 August 1993)

Electronic trajectories in a free-electron laser consisting of a helical wiggler magnetic field and a uniform guide field are studied using a three-dimensional approach. It is well known that, to any orbit, there corresponds two conserved quantities. One is the energy, while the second, which we call P_z, is a consequence of the screw-displacement symmetry of the wiggler field. Depending on the value of P_z, the Hamiltonian, after a canonical transformation, may be shown to have a fixed point which represents steady motion on an axially centered helical path of the same pitch as the wiggler. Expanding the Hamiltonian about the fixed point and retaining only quadratic terms, we obtain an approximate description of the motion in terms of two harmonic oscillators whose characteristic frequencies and normal modes are determined by the value of P_z. Despite the simplicity of the dynamics, the nonlinear relations which link our oscillator variables to the Cartesian coordinates and velocities provide a detailed description of the complex behavior of the latter. Provided that the magnitudes of the oscillator amplitudes are not too large, our method yields trajectories in close agreement with those computed numerically. Among the features encountered is that in both group I, and with reversed-field operation, one of the frequencies is negative, while in group-II operation a repulsion of the frequencies at a pseudocrossing leads to highly perturbed trajectories when the wiggler frequency is approximately half the cyclotron frequency. In favorable circumstances, which we specify, the transverse motion is accurately described by a superposition of three circular motions; one corresponds to the fixed point, the second to the cyclotronic motion, while the third is a very slow motion of the center of gyration. The axial velocity then shows ripple at approximately the difference of cyclotron and wiggler frequencies. The spontaneous-forward-emission spectrum peaks at the Lorentz-boosted wiggler and cyclotron frequencies. Under less favorable circumstances, the motion we predict is more complicated, and the resulting forward-emission spectrum rather complex.

PACS number(s): 41.60.Cr

I. INTRODUCTION

A commonly used configuration for a free-electron laser (FEL) consists of a helicoidally wound bifilar coil, which provides an on-axis wiggler magnetic field of a given handedness or chirality, and whose step size we denote by λ_w. A solenoid, which coaxially encloses the wiggler coil, provides, in addition, a uniform axial guide magnetic field B_0 in the z direction. In the limit in which the magnets are infinitely long, the trajectory of an electron in the resulting field is described by two conserved quantities. One is the energy, due to the static nature of the magnetic field, while the second, which we call P_z (it is not simply the z component of momentum), is related to the invariance under a combined rotation of angle $\Delta\phi$ about the axis of symmetry and a translation of length $\Delta z=\lambda_w\Delta\phi/2\pi$ along the axis of symmetry. To the best of our knowledge, no third conserved quantity has been found; hence the problem is not exactly integrable. Considerable numerical and analytic effort has been devoted to the study of the trajectories, and a large amount of experimental results on such FEL's has been accumulated [1–5].

A simplified treatment exists in which the inevitable dependence of the wiggler field on the transverse spatial variables is neglected [the one-dimensional (1D) approximation]. In this approximation the problem becomes exactly integrable in terms of elliptic functions, but interest has mainly centered on the particular case of steady motion, where the electron's orbit is a helix whose pitch is the same as that of the wiggler field, and for which the longitudinal and transverse velocities v_z and $v_\perp$ are constant. These velocities are constrained by the relation

$$\gamma v_\perp=\frac{\gamma v_z\Omega_w}{|\gamma v_z k_w-\Omega_0|}\ , \tag{1}$$

where γ is the electron's energy in units of mc^2, where m is the mass of the electron, $k_w=2\pi/\lambda_w$ is the wiggler wave number, and Ω_w and Ω_0 denote the nonrelativistic cyclotron frequencies eB_w/mc and eB_0/mc, respectively. If the longitudinal velocity could be made to approach the value $\Omega_0/(\gamma k_w)$, then the transverse velocity would be very large, a favorable situation called the gyroresonance. The radius ρ of the helical orbit is related to the velocities by $k_w\rho=v_\perp/v_z$.

Although the 1D approximation provides insight, a 3D treatment is required to investigate the nature of the

*Permanent address: Centre d'Etudes Scientifiques et Techniques d'Aquitaine, Commissariat à l'Energie Atomique, Le Barp, France.

gyroresonance. In contrast to the 1D approximation, the system is not exactly integrable, but again a particular case of steady helical motion does exist. However, the symmetry axis of these helical orbits, which may be freely chosen in the 1D approximation, must now coincide with the axis of the wiggler field. In Ref. [1], Freund and Ganguly have presented a thorough description of these orbits, and of the perturbed trajectories which remain in their vicinities. They establish the essential relation between the longitudinal and transverse velocities which replaces Eq. (1). Writing $|\lambda| = v_\perp / v_z$, they find

$$\gamma v_z k_w = \Omega_0 - 2\Omega_w (1+\lambda^{-2}) I_1(\lambda) , \tag{2}$$

where I_1 denotes the modified Bessel function of order 1. Positive λ corresponds to trajectories of group II, with $v_z < \Omega_0/(\gamma k_w)$, whereas negative λ corresponds to trajectories of group I, with $v_z > \Omega_0/(\gamma k_w)$. If one expands the right-hand side to lowest order in λ, Eq. (1) is recovered. One notes also that if λ is sufficiently small and positive, v_z becomes negative, or antiparallel to the axial field. This is the reversed-field configuration, which has been studied both theoretically and experimentally.

Our interest in this problem was kindled by some unexpected results found in a numerical study of the electron trajectories in such a magnetic field. The study concerned the propagation of electrons of kinetic energy 1.5 MeV in a wiggler of step size 12 cm, with axial fields in the range 0.5–1.2 T, and wiggler fields typically an order of magnitude smaller [6]. For some values of the magnetic fields, the numerically generated trajectories resembled the sought-for-helical orbits, with the longitudinal velocity showing only a small (1%) ripple and the transverse Cartesian velocities oscillating regularly with the wiggler frequency $k_w v_z$. However, for other choices of the fields, trajectories which displayed significant (10%) fluctuations in the longitudinal velocity as well as irregular oscillations in the transverse velocities were observed. Because the successful generation of radiation requires coherence between the electron's orbit and a circularly polarized electromagnetic wave, such large fluctuations in longitudinal velocity are highly undesirable. In order to understand their origin, we have recast the problem in a Hamiltonian formalism, with the double aim of eliminating the degree of freedom corresponding to the conserved quantity P_z related to the screw-displacement symmetry, and of utilizing the freedom to make canonical transformations which simplify the Hamiltonian. The resulting Hamiltonian, which we call H, obtained after some manipulations, has the remarkable property of possessing a fixed point. By this, we mean a point in phase space where the four derivatives of H with respect to the generalized momenta and coordinates are zero. If the electron were exactly at the fixed point, it would stay there indefinitely, but this fixed point in phase space does not correspond to an immobile electron in real space. Instead, it is just the ideal helical motion that all experiments aim to realize. We then perform a Taylor-series expansion of the Hamiltonian around the fixed point, keeping only second-order terms. The resulting truncated Hamiltonian is then diagonalized by a final canonical transformation, yielding two uncoupled harmonic oscillators. The resulting system, although not exact, is integrable, and does provide a satisfactory description of those trajectories that are not too far away from the ideal orbits.

Since our approach essentially involves perturbing the ideal helical motion, it is appropriate to compare our results to those presented by Freund and Ganguly in Ref. [1]. First we note that our expression for the squares of the frequencies of the oscillators agrees precisely with their's, thereby confirming their results. In addition, we determine the signs of the frequencies, one of which is negative in group-I and group-II reversed-field operation. Negative frequencies mean that increasing the corresponding amplitude lowers the energy, a rather counterintuitive result. In our approach, it is clear that the key role in calculating the orbit is played by the conserved quantity we call P_z. Given the five independent initial conditions (e.g., the values of x, y, and the three components of velocity at $z=0$), we extract the value of P_z that characterizes the true trajectory throughout its length. Using only this quantity, the appropriate fixed point is determined, and the corresponding eigenfrequencies and eigenvectors of the oscillators are computed. The four remaining initial conditions then provide the initial magnitudes and phases of our oscillator amplitudes. The magnitudes are conserved quantities along our approximate trajectories, the phases are linear functions of time, and the position and velocity of the electron may be computed easily at any time. The price we must pay is that the true electron energy, as calculated from the initial velocity, does not precisely agree with that of the truncated Hamiltonian. If the discrepancy between the true energy and our approximate energy is small, and it is easily computed, our calculated trajectories remain quite close to those generated numerically. The motion we compute is somewhat more complicated than that predicted in the approach of Ref. [1], essentially because we keep track of terms which are second order in the perturbation. After transforming back to ordinary position and velocity, we find second-order corrections that behave as sums and differences of our oscillator frequencies. Such behavior is often clearly visible in the numerically calculated trajectories.

Using the trajectories we compute in our model, it is straightforward to calculate the spontaneous-emission spectrum (in the z direction) for a given electron, exactly in the case of free space (see the Appendix), and approximately for the case of emission in a cylindrical wave guide [7]. According to Madey's theorem [8], the small-signal gain is related to the derivative of the spontaneous-emission spectrum. In contrast to the quasimonochromatic spectrum of the ideal helical motion, our model predicts in general a rather complex spectrum, caused by the presence of the oscillations in the transverse variables as well as by the nonuniform longitudinal velocity.

Finally, our approach provides a simple explanation for the irregular motion occasionally seen in the numerical trajectories, and which motivated our investigation. The phenomenon occurs when the two eigenfrequencies

attempt to "cross" one another as some parameter, e.g., the axial field, is varied. As is well known from quantum mechanics, the frequencies "repel" each other, and the eigenvectors display rapid variation when this occurs. A certain number of quantities which elsewhere behave quite smoothly exhibit violent variations, which considerably perturb the trajectories. This only occurs for the group-II trajectories in the terminology of Ref. [1], but it does occur in a region sufficiently far away from the well-known instabilities to be of interest for FEL operation. The existence of this perturbed region, and the corresponding interdiction to operate the FEL nearby, is the principal result of this investigation.

The approximation we present is applicable to both the group-I and group-II modes discussed in Ref. [1], and also to the reversed-field mode of operation that has recently been studied experimentally [4] and theoretically [9]. We have not considered the effects of keeping cubic terms in the expansion of the Hamiltonian. Such terms will be important whenever the oscillator amplitudes are large, and their presence would produce such effects as amplitude-dependent frequency shifts, mode locking, and other such complications displayed by nonlinear coupled oscillators.

Even when the amplitudes are not large, the cubic and higher-order terms may become troublesome if the ratio of the frequencies approaches a rational fraction of "small integers" [10]. Our method does allow us to locate these potentially dangerous situations, in particular, the ratio 2:1. When the frequencies are approximately in this ratio, some neglected cubic terms will be almost constant in time, and these may cause the oscillator amplitudes to vary with time. If this occurs, our simple picture of fixed amplitude oscillation is not valid.

The paper is organized as follows. The Hamiltonian formalism and our dynamical variables are introduced in Sec. II. The conditions under which fixed points exist and their relation to the conserved quantity P_z are discussed in Sec. III. In Sec. IV we present the truncated quadratic Hamiltonian, illustrate the behavior of the amplitudes and frequencies, and give explicit expressions for the position and velocity as functions of time. In Sec. V we show how our results, when some approximations are valid, provide a simple description of the electronic orbits. Section VI presents our conclusions. Details of the computation of the oscillator amplitudes and the spectrum of spontaneous-forward-direction emission are given in the Appendix. Preliminary results of this investigation may be found in the dissertation of one of us (J.L.R.), together with a detailed comparison of orbits computed using our method and standard numerical integration [11].

II. HAMILTONIAN FORMALISM FOR THE HELICAL WIGGLER WITH AN AXIAL MAGNETIC FIELD

A. Magnetic field and vector potential

The magnetic field may be written as (in cylindrical coordinates ρ,ϕ,z)

$$\mathbf{B}(\mathbf{x})=B_z\hat{\mathbf{e}}_z+B_\rho\hat{\mathbf{e}}_\rho+B_\phi\hat{\mathbf{e}}_\phi \ , \tag{3}$$

where the components are given by [12]

$$B_\rho=2B_w I_1'(k_w\rho)\sin(\phi-k_w z) \ , \tag{4a}$$

$$B_\phi=2B_w[I_1(k_w\rho)/k_w\rho]\cos(\phi-k_w z) \ , \tag{4b}$$

$$B_z=B_0-2B_w I_1(k_w\rho)\cos(\phi-k_w z) \ . \tag{4c}$$

In these expressions I_1 denotes the modified Bessel function of order 1, I_1' its derivative, B_0 is the constant axial guide field, B_w is the on-axis wiggler magnetic field, and k_w is related to the wiggler period λ_w by $k_w=2\pi/\lambda_w$. By choosing appropriately the origin and the direction of the z axis, one may, without loss of generality, choose B_w and B_0 to be positive. The chirality or handedness of the wiggler field is determined by the sign of k_w, which we suppose positive. The magnetic field may be written as the curl of the vector potential as follows:

$$\mathbf{B}(\mathbf{x})=\nabla\times\mathbf{A}(\mathbf{x}) \ , \tag{5}$$

and one may verify that the following vector potential yields the correct magnetic field:

$$A_z=0 \ , \tag{6a}$$

$$A_\rho=-2(B_w/k_w)[I_1(k_w\rho)/k_w\rho]\sin(\phi-k_w z) \ , \tag{6b}$$

$$A_\phi=B_0\rho/2-2(B_w/k_w)I_1'(k_w\rho)\cos(\phi-k_w z) \ . \tag{6c}$$

Because the vector potential has z component zero, one may succinctly represent it in terms of the complex quantity

$$A_x+iA_y=i[B_0(x+iy)/2-(B_w/k_w)e^{ik_w z}J] \ , \tag{7}$$

where the function of ρ,ϕ,z we call J is specified by

$$J=I_0(k_w\rho)+I_2(k_w\rho)e^{2i(\phi-k_w z)} \ , \tag{8}$$

where I_0 and I_2 denote modified Bessel functions of order 0 and 2, respectively. Note that if the quantity $(\phi-k_w z)$ has the value 0 (modulo π), then J is real and has the positive value $2I_1'(k_w\rho)$.

B. Hamiltonian description

The Hamiltonian for a particle of charge $-e$ is obtained from the free-particle Hamiltonian by the usual substitution [13]

$$\mathbf{p}\rightarrow\mathbf{p}+e\,\mathbf{A}(\mathbf{x})/c \ ,$$

where c is the speed of light. One obtains the Hamiltonian

$$H(\mathbf{p},\mathbf{x})=\{m^2c^4+[c\mathbf{p}+e\,\mathbf{A}(\mathbf{x})]^2\}^{1/2} \ , \tag{9}$$

where $\mathbf{p}$ is the canonical momentum, and m is the mass of the charged particle. The standard equations then apply:

$$\frac{dx_i}{dt}\equiv v_i=\frac{\partial H}{\partial p_i}, \quad \frac{dp_i}{dt}=-\frac{\partial H}{\partial x_i} \ , \tag{10}$$

where x_i, v_i, and p_i denote the Cartesian coordinates of position, velocity, and canonical momentum, respective-

ly, and t denotes time. Explicitly, one finds for the velocities

$$\frac{dz}{dt}=\frac{\partial H}{\partial p_z}=\frac{c^2 p_z}{H} , \tag{11a}$$

$$\frac{d(x+iy)}{dt}=\left[\frac{\partial}{\partial p_x}+i\frac{\partial}{\partial p_y}\right]H$$

$$=\frac{c}{H}[c(p_x+ip_y)+e(A_x+iA_y)] , \tag{11b}$$

which may also be written in terms of β_i as

$$\beta_z=\frac{cp_z}{H} , \tag{12a}$$

$$\beta_x+i\beta_y=[c(p_x+ip_y)+e(A_x+iA_y)]/H , \tag{12b}$$

where $\beta_i=v_i/c$.

C. Dimensionless variables and a canonical transformation

If we introduce dimensionless variables as follows:

$$\hat{H}=H/mc^2,\ \hat{p}_i=p_i/mc,\ \hat{x}_i=k_w x_i,\ \hat{t}=ck_w t ,$$

then Hamilton's equations remain valid for the careted variables. We then introduce two new dimensionless complex dynamical variables a and b, defined in terms of the canonical momenta and position variables by [14]

$$a=\left[\frac{k_w}{2eB_0 m}\right]^{1/2}\left[p_y-ip_x+\frac{eB_0}{2c}(x+iy)\right]e^{-ik_w z} , \tag{13a}$$

$$b=\left[\frac{k_w}{2eB_0 m}\right]^{1/2}\left[p_x-ip_y+i\frac{eB_0}{2c}(x-iy)\right]e^{ik_w z} . \tag{13b}$$

The Poisson brackets of these variables are given by

$$\{a,a^*\}=\{b,b^*\}=ik_w/mc , \tag{14a}$$

$$\{a,b\}=\{a,b^*\}=0 , \tag{14b}$$

$$\{a,\hat{p}_z\}=-ik_w a/mc , \tag{14c}$$

$$\{b,\hat{p}_z\}=ik_w b/mc , \tag{14d}$$

which shows that they are not dynamically independent of the z component of momentum. However, one may define a new momentum

$$P_z=\hat{p}_z+|a|^2-|b|^2 , \tag{15}$$

such that

$$\{a,P_z\}=\{b,P_z\}=0 , \tag{16}$$

while

$$\{\hat{z},P_z\}=k_w/mc . \tag{17}$$

The new variables are thus obtained by a canonical transformation from the original Cartesian position and momentum variables.

The usual variables are then related to a and b as follows:

$$x+iy=(2/\hat{\Omega}_0)^{1/2}(a+ib^*)e^{ik_w z}/k_w , \tag{18a}$$

$$p_x+ip_y=imc(\hat{\Omega}_0/2)^{1/2}(a-ib^*)e^{ik_w z} , \tag{18b}$$

where the dimensionless nonrelativistic cyclotron frequency

$$\hat{\Omega}_0=eB_0/mc^2k_w \tag{19}$$

has been introduced. Given the values of the transverse position and momenta at a fixed value of z, one may use these expressions to obtain initial values of a and b. From Eq. (18a) it follows that

$$\phi-\hat{z}=\arg(a+ib^*) , \tag{20a}$$

$$k_w\rho\equiv\hat{\rho}=(\hat{\Omega}_0/2)^{-1/2}\mathrm{mod}(a+ib^*) , \tag{20b}$$

where arg and mod denote the argument and the modulus of a complex number, and $\hat{\rho}$ is the dimensionless radial coordinate. Using these relations one may write the complex quantity J as

$$J=I_0(\hat{\rho})+I_2(\hat{\rho})\frac{(a+ib^*)}{(a^*-ib)} , \tag{21}$$

and notice that it depends only on a and b. We may also write

$$p_x+ip_y+\frac{e}{c}(A_x+iA_y)=imc[(2\hat{\Omega}_0)^{1/2}a-\hat{\Omega}_w J]e^{i\hat{z}} , \tag{22}$$

where $\hat{\Omega}_w=eB_w/(mc^2k_w)$.

Hamilton's equations of motion for the dimensionless variables may now be written as

$$\frac{d\hat{z}}{d\hat{t}}=\frac{\partial\hat{H}}{\partial P_z},\quad \frac{dP_z}{d\hat{t}}=-\frac{\partial\hat{H}}{\partial\hat{z}} , \tag{23a}$$

$$\frac{da}{d\hat{t}}=i\frac{\partial\hat{H}}{\partial a^*},\quad \frac{db}{d\hat{t}}=i\frac{\partial\hat{H}}{\partial b^*} , \tag{23b}$$

where the dimensionless Hamiltonian is

$$\hat{H}(\hat{z},P_z,a,b)=\{1+[P_z-|a|^2+|b|^2]^2$$

$$+2\hat{\Omega}_0|a-\hat{\Omega}_w J/(2\hat{\Omega}_0)^{1/2}|^2\}^{1/2} . \tag{24}$$

The function J depends only on the complex variables a and b, which means that the Hamiltonian is independent of the variable $\hat{z}$; hence P_z is a conserved quantity. It is identical, except for a factor mc, to the conserved quantity introduced by Freund and Ganguly in Ref. [1]. The origin of this conserved quantity is the screw-displacement symmetry of the helical magnetic field. A rotation about the z axis combined with a translation along the axis such that $\phi-k_w z$ is unchanged is clearly a symmetry of the Hamiltonian. As we shall show, in our approach this conserved quantity plays a crucial role in the calculation of the trajectories.

The quantity $d\hat{z}/d\hat{t}$, which is simply β_z, may be then written as

$$\frac{d\hat{z}}{d\hat{t}}=(P_z-|a|^2+|b|^2)/\hat{H} \ , \tag{25}$$

which illustrates how the longitudinal velocity depends on the moduli of the dynamical variables a and b.

D. Integrability of the one-dimensional approximation

It is worth noting that the 1D approximation can easily be obtained in the present treatment. If, in the Hamiltonian, the function J is replaced by the first term in its Taylor-series expansion, $J=1$, one finds

$$\hat{H}_{1D}(a,b)=\{1+[P_z-|a|^2+|b|^2]^2 +2\hat{\Omega}_0|a-\hat{\Omega}_w/(2\hat{\Omega}_0)^{1/2}|^2\}^{1/2} \ , \tag{26}$$

which is independent of the phase of the complex dynamical variable b. Consequently, the magnitude of b is conserved, and one can even show that $be^{-i\hat{z}}$ is a conserved complex quantity. Writing the variable a in the form $|a|e^{i\eta}$, one may solve for the phase η as a function of the modulus, obtaining

$$\cos\eta=\frac{1+(P_z-|a|^2+|b|^2)^2+2\hat{\Omega}_0|a|^2+\hat{\Omega}_w^2-\hat{H}_{1D}^2}{\hat{\Omega}_w|a|(8\hat{\Omega}_0)^{1/2}} \ , \tag{27}$$

and then insert this into Hamilton's equation

$$\frac{d|a|^2}{d\hat{t}}=-\frac{\partial\hat{H}_{1D}}{\partial\eta}=\frac{-[\hat{\Omega}_w|a|(2\hat{\Omega}_0)^{1/2}\sin\eta]}{\hat{H}_{1D}} \ . \tag{28}$$

It follows from Eq. (27) that the right-hand side of Eq. (28) is the square root of a quartic polynomial in the variable $|a|^2$. A discussion of the explicit integration of this equation in terms of the Weierstrassian elliptic functions is given, for example, by Whittaker and Watson [15]. The 1D approximation is thus exactly integrable, in contrast to the full 3D Hamiltonian. This fact has been known for some time [16], but we find the derivation using our formalism rather simple.

III. FIXED POINT OF THE HAMILTONIAN

The task of determining the fixed point for a given value of P_z is simplified by the fact that our Hamiltonian is invariant under the discrete transformation

$$a\leftrightarrow a^*, \quad b\leftrightarrow -b^* \ .$$

From this, it follows that the quantities $(a-a^*)$ and $(b+b^*)$ can occur in the Taylor-series expansion of the Hamiltonian only in the combinations $(a-a^*)^2$, $(b+b^*)^2$, and $[(a-a^*)(b+b^*)]$. If a is real and b is imaginary, the first derivatives with respect to $(a-a^*)$ and $(b+b^*)$ are therefore necessarily zero. This leaves us with the much simpler problem of finding two real quantities a_f and b_f, where $a=a_f$ and $b=ib_f$, such that the first derivatives of $\hat{H}$ with respect to $(a+a^*)$ and $(b-b^*)$ vanish. We thus consider the Hamiltonian to be a function of these two real variables a_f and b_f, and impose the vanishing of both derivatives

$$\frac{\partial\hat{H}}{\partial a_f}=0, \quad \frac{\partial\hat{H}}{\partial b_f}=0 \ . \tag{29}$$

One way to solve the problem is to notice that the condition

$$\frac{\partial\hat{H}}{\partial a_f^2}+\frac{\partial\hat{H}}{\partial b_f^2}=0 \ , \tag{30}$$

does not depend on the value of the conserved quantity P_z, and thus defines a curve in the (a_f,b_f) plane which depends only on the magnetic-field parameters. The simplest way to describe this curve is to specify a_f and b_f in terms of a real parameter $\hat{\rho}_f$, as follows from Eq. (20b),

$$a_f+b_f=(\hat{\Omega}_0/2)^{1/2}\hat{\rho}_f \ , \tag{31}$$

and then to verify that Eq. (30) is satisfied if

$$b_f=\hat{\Omega}_w(8\hat{\Omega}_0)^{-1/2}\hat{\rho}_f[3I_1(\hat{\rho}_f)+I_3(\hat{\rho}_f)] \ , \tag{32}$$

where I_1 and I_3 denote modified Bessel functions. Note that b_f is an even function of $\hat{\rho}_f$. The quantity $|\hat{\rho}_f|$ is the scaled radius, i.e., $k_w\rho$, of the ideal helical trajectory.

The next step is to determine the value of the parameter $\hat{\rho}_f$. To accomplish this, one replaces a_f and b_f using Eqs. (31) and (32), and imposes

$$\frac{\partial\hat{H}}{\partial\hat{\rho}_f}=0 \ , \tag{33}$$

which yields, after using some identities among Bessel functions, the relation

$$P_z-a_f^2+b_f^2=\hat{\Omega}_0-2\hat{\Omega}_w(1+\hat{\rho}_f^{-2})I_1(\hat{\rho}_f) \ . \tag{34}$$

The left-hand side of this equation is the scaled z component of linear momentum at the fixed point, which may also be written as $(\gamma\beta_z)_f$. If we allow for the fact that the variable $\hat{\rho}_f$ may have either sign, we recognize our Eq. (2), which was established in Ref. [1]. They divided the steady motion trajectories into two groups: group I, containing those with $\beta_z>\hat{\Omega}_0/\gamma$, and group II, containing those with $\beta_z<\hat{\Omega}_0/\gamma$. Since the modified Bessel function I_1 is positive for positive arguments and negative for negative arguments, we see that the groups I and II correspond to negative and positive values of $\hat{\rho}_f$, respectively. In addition, we note that for sufficiently small positive values of $\hat{\rho}_f$, the right-hand side becomes negative, which means that the longitudinal velocity is opposite to the direction of the axial guide field.

In preference to Eq. (34) we shall use

$$P_z=\hat{\Omega}_0(1+\hat{\rho}_f^2/2) -\hat{\Omega}_w[(4\hat{\rho}_f^{-2}+4+3\hat{\rho}_f^2)I_1(\hat{\rho}_f)+\hat{\rho}_f^2I_3(\hat{\rho}_f)]/2 \ , \tag{35}$$

which relates the conserved quantity P_z to the parameter $\hat{\rho}_f$. This relation is obtained from Eq. (34) simply by adding the quantity $(a_f^2-b_f^2)$ both sides, and using Eqs. (31) and (32) to express a_f and b_f in terms of $\hat{\rho}_f$. Our reason for using Eq. (35) instead of (34) is that an arbitrary trajectory has a conserved momentum P_z, whereas only the ideal helical trajectories have a constant β_z. Therefore,

although the two equations contain the same information relating the scaled radius $|\hat{\rho}_f|$ of the ideal helical trajectory to $\gamma\beta_z$, Eq. (35) allows one to associate a fixed point (provided certain conditions are met) with a completely arbitrary trajectory. Given the fixed point, the Hamiltonian may be expanded in a power series in the variables $(a-a_f)$ and $(b-ib_f)$ and their complex conjugates. If we keep only quadratic terms, the resulting approximate Hamiltonian may be diagonalized by a subsequent linear canonical transformation, yielding two uncoupled harmonic oscillators. The frequencies and coefficients of the normal modes of vibration depend only on the value of the quantity $\hat{\rho}_f$ at the fixed point. Provided that the amplitudes of the oscillation are sufficiently small, a quantitative description of the trajectory is obtained.

The relation between the conserved momentum P_z and the parameter $\hat{\rho}_f$ is illustrated in Figs. 1(a) and 1(b), for two different values of the ratio B_w/B_0, 0.1 and 0.2, respectively. We plot $P_z/\hat{\Omega}_0$, which depends only on $\hat{\rho}_f$ and the ratio B_w/B_0, as a function of $\hat{\rho}_f$ for $-2<\hat{\rho}_f<2$. For negative values of $\hat{\rho}_f$, the curve has a roughly U-shaped form, which corresponds to the group-I trajectories. For positive $\hat{\rho}_f$ the curve has an inverted U shape and the trajectories belong to group II. Note that if $\hat{\rho}_f$ is sufficiently small and positive, $P_z/\hat{\Omega}_0$ becomes negative, which corresponds to the reversed-field configuration in which the directions of the beam and axial magnetic field are antiparallel. It is apparent from these curves that for a given value of $P_z/\hat{\Omega}_0$, the fixed points occur in pairs. Both fixed points correspond to uniform helical motion, but subsequent analysis will show that the fixed point with the larger value of $|\hat{\rho}_f|$ is, in fact, unstable, while that of smaller $|\hat{\rho}_f|$ is stable. The points labeled $S_{\rm I}$ represent the minimum allowed values of $P_z/\hat{\Omega}_0$ for group-I trajectories, while those labeled $S_{\rm II}$ correspond to the maximum allowed values of $P_z/\hat{\Omega}_0$ for group-II trajectories. These points, as we shall show, separate the stable from the unstable fixed points. The limiting situation, in which the pairs coalesce (at the maximum or the minimum) corresponds to a zero frequency and hence to the limit of stable motion. Inspection of Fig. 1(a) reveals that the value of $P_z/\hat{\Omega}_0$ at $S_{\rm I}$ is less than that at $S_{\rm II}$; hence there is a range of $P_z/\hat{\Omega}_0$ for which two stable fixed points exist, one in group I and the other in group II. In contrast, one sees in Fig. 1(b) that $P_z/\hat{\Omega}_0$ at $S_{\rm I}$ is greater than that at $S_{\rm II}$; hence there is a range of $P_z/\hat{\Omega}_0$ for which no fixed point exists. Electrons having values of $P_z/\hat{\Omega}_0$ in this forbidden gap cannot propagate in the magnetic field. Inevitably they spiral out in the transverse directions, converting longitudinal into transverse energy, until they encounter the confining transverse structure.

In Fig. 2 we show the values of $P_z/\hat{\Omega}_0$ at the extremal points $S_{\rm I}$ and $S_{\rm II}$ as a function of the ratio B_w/B_0. Points in the $(B_w/B_0, P_z/\hat{\Omega}_0)$ plane that lie above the curve labeled I min correspond to fixed points of group I and therefore the curve corresponds to minimal values of $P_z/\hat{\Omega}_0$. Similarly, points situated below the curve labeled II max correspond to fixed points of group II, and the curve to maximal values of $P_z/\hat{\Omega}_0$. These limiting curves intersect at the approximate point $B_w/B_0=0.118$, $P_z/\hat{\Omega}_0=1.433$, where the forbidden gap (horizontal hatching) starts. If $B_w/B_0>0.118$ then there exists a forbidden range of $P_z/\hat{\Omega}_0$ values, whereas if $B_w/B_0<0.118$ then there exists at least one stable fixed point for any value of $P_z/\hat{\Omega}_0$. In the overlap region (vertical hatching) which lies above I min and below II max, there are two stable fixed points for a given value of $P_z/\hat{\Omega}_0$. In this situation, knowledge of P_z alone does not determine the stable ideal helical trajectory, since there are two of them. The Hamiltonian may be expanded about either stable fixed point, but only for one (at best) is the energy of the particle approximately equal to the value of the Hamiltonian at the fixed point. It should be noted that for values of $B_w/B_0>0.45$, the only allowed fixed point in group II is of the reversed-field type.

Although it is easy to evaluate P_z once $\hat{\rho}_f$ is given, the inverse problem, finding $\hat{\rho}_f$ when P_z is known, can only be solved numerically. However, provided the value of P_z is not in the gap, one may use Newton's method to find the appropriate value (or values) of $\hat{\rho}_f$. In what follows, we shall present our results in terms of functions of $\hat{\rho}_f$, but it should be understood that $\hat{\rho}_f$ is determined by the conserved quantity P_z, which is an observable proper-

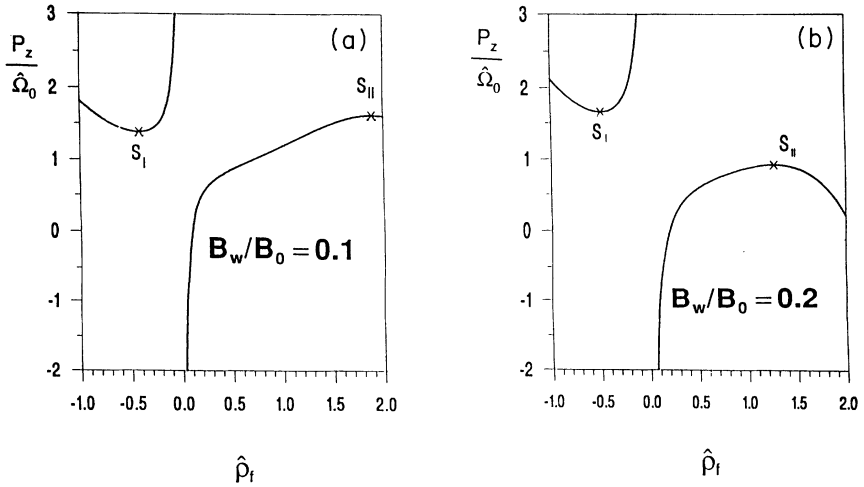

FIG. 1. (a) The quantity $P_z/\hat{\Omega}_0$ as a function of $\hat{\rho}_f$, with the ratio $B_w/B_0=0.1$. Negative values of $\hat{\rho}_f$ correspond to group I, positive to group II, while the reversed-field configuration corresponds to negative values of P_z. The limits of the stability region, between which the slope is positive, are indicated by $S_{\rm I}$ and $S_{\rm II}$. For any value of $P_z/\hat{\Omega}_0$ at least one stable fixed point exists. (b) Same as in (a) but with the ratio $B_w/B_0=0.2$. There exist values of $P_z/\hat{\Omega}_0$ for which no stable fixed point exists.

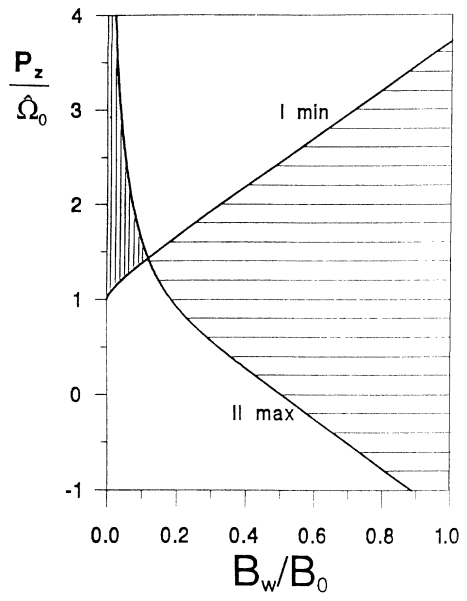

FIG. 2. Regions of stability in the plane $(B_w/B_0,\ P_z/\hat{\Omega}_0)$. For group-I operation the point must lie above the curve labeled I min, whereas for group-II operation the point must lie below the curve labeled II max. The horizontally-cross-hatched area is forbidden, while at any point in the vertically-cross-hatched area two distinct stable fixed points exist.

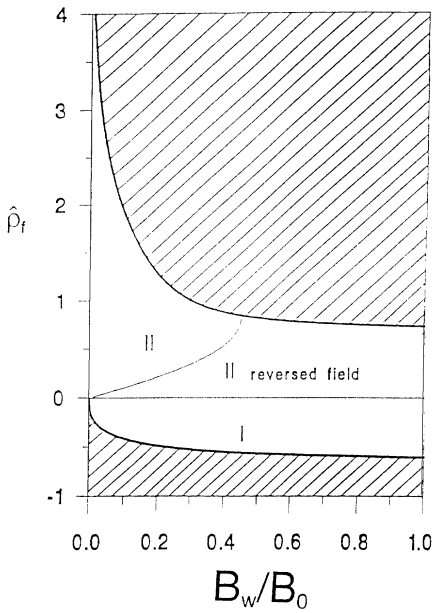

FIG. 3. Regions of stability in the plane $(B_w/B_0,\ \hat{\rho}_f)$. The cross-hatched areas are forbidden, while the allowed regions for group-I, group-II normal, and reversed-field operation are indicated.

ty of the real trajectory.

Once the fixed point has been determined, the corresponding longitudinal momentum $(\gamma\beta_z)_f$ at the fixed point is given by Eq. (34), while the corresponding transverse momentum $(\gamma\beta_\perp)_f$ is given by

$$(\gamma\beta_\perp)_f=|\hat{\rho}_f|(\gamma\beta_z)_f\ , \tag{36a}$$

and the energy γ_f at the fixed point is specified by

$$\gamma_f^2=1+(1+\hat{\rho}_f^2)(\gamma\beta_z)_f^2\ . \tag{36b}$$

We also introduce, for future use, the ratio $(\gamma\beta_z)_f/\hat{\Omega}_0$, which we call r_f. It is a function only of the ratio B_w/B_0 and $\hat{\rho}_f$, namely,

$$\begin{aligned} r_f &\equiv(\gamma\beta_z)_f/\hat{\Omega}_0 \\ &=1-2(B_w/B_0)(1+\hat{\rho}_f^{-2})I_1(\hat{\rho}_f)\ . \end{aligned} \tag{37}$$

This quantity is >1 for group-I and <1 for group-II fixed points. It will prove useful in the next section, where we examine the behavior of trajectories that are in the neighborhood of the ideal helical trajectories.

In Fig. 3 we show the regions of the $(B_w/B_0,\hat{\rho}_f)$ plane for which stable fixed points exist. The cross-hatched regions are forbidden, while group-II and group-I fixed points correspond to positive and negative values of $\hat{\rho}_f$, respectively. The thin line separates the group-II normal and reversed-field fixed points. We point out that only for group-II normal fixed points can large values of $|\hat{\rho}_f|$ be obtained, and this only when the ratio B_w/B_0 is small, which implies either large axial or small wiggler fields.

IV. QUADRATIC APPROXIMATION TO THE HAMILTONIAN

A. Characteristic frequencies

If the value of the conserved quantity P_z is such that a fixed point of the Hamiltonian exists, a natural next step is to expand the Hamiltonian in a Taylor series about the fixed point. By definition, the first-order terms vanish, and one may write

$$\hat{H}(P_z,a,b)=\hat{H}(P_z,a_f,ib_f)+\hat{H}_Q+\cdots\ , \tag{38}$$

where a_f and ib_f are the values of a and b at the fixed points, $\hat{H}_Q$ is the quadratic part of the Hamiltonian, and higher terms start with expressions cubic in the deviation from the fixed point. We define explicitly

$$\xi^1=\mathrm{Re}(a)-a_f\ , \tag{39a}$$

$$\xi^2=\mathrm{Im}(a)\ , \tag{39b}$$

$$\xi^3=\mathrm{Re}(b)\ , \tag{39c}$$

$$\xi^4=\mathrm{Im}(b)-b_f \tag{39d}$$

(here Re and Im denote real and imaginary parts, respectively). If we then call

$$\hat{H}_{kl}=\frac{\partial^2\hat{H}}{\partial\xi^k\partial\xi^l}\ , \tag{40}$$

where the second derivatives of the Hamiltonian are evaluated at the fixed point, we may write the quadratic Hamiltonian as

$$\hat{H}_Q=\frac{1}{2}\sum_{k,l=1}^{4}\xi^k\xi^l\frac{\partial^2\hat{H}}{\partial\xi^k\partial\xi^l}\ . \tag{41}$$

Although one would normally expect to find ten terms in the quadratic approximation, the discrete symmetry of the Hamiltonian allows one to reduce the number of terms to six, which facilitates the subsequent analysis. Taking into account the discrete symmetry, we obtain the matrix

$$\begin{bmatrix} \hat{H}_{11} & 0 & 0 & \hat{H}_{14} \\ 0 & \hat{H}_{22} & \hat{H}_{23} & 0 \\ 0 & \hat{H}_{23} & \hat{H}_{33} & 0 \\ \hat{H}_{14} & 0 & 0 & \hat{H}_{44} \end{bmatrix} .$$

Explicit expressions for the six quantities $\hat{H}_{kl}$ are given in the Appendix.

We next look for a new dynamical variable A, which is linear in the variables ξ^k, and has the following simple Poisson bracket with the quadratic Hamiltonian:

$$\{A,\hat{H}_Q\}=i(k_w/mc)\hat{\Omega}A \ , \tag{42}$$

where $\hat{\Omega}$ is a dimensionless frequency to be determined. This is simply a linear eigenvalue problem, whose solution is easily found. If we write

$$A=\eta_1\xi^1-\eta_4\xi^4+i(\eta_2\xi^2+\eta_3\xi^3) \ , \tag{43}$$

where the η_k are unknown coefficients, we obtain the matrix equations

$$2\hat{\Omega}\begin{bmatrix}\eta_1\\ \eta_4\end{bmatrix}=\begin{bmatrix}\hat{H}_{11} & -\hat{H}_{14}\\ -\hat{H}_{14} & \hat{H}_{44}\end{bmatrix}\begin{bmatrix}\eta_2\\ \eta_3\end{bmatrix} , \tag{44a}$$

$$2\hat{\Omega}\begin{bmatrix}\eta_2\\ \eta_3\end{bmatrix}=\begin{bmatrix}\hat{H}_{22} & \hat{H}_{23}\\ \hat{H}_{23} & \hat{H}_{33}\end{bmatrix}\begin{bmatrix}\eta_1\\ \eta_4\end{bmatrix} , \tag{44b}$$

which may be combined to yield the simple result

$$\begin{bmatrix}\hat{H}_{11}\hat{H}_{22}-\hat{H}_{14}\hat{H}_{23}-4\hat{\Omega}^2 & \hat{H}_{23}\hat{H}_{44}-\hat{H}_{14}\hat{H}_{22}\\ \hat{H}_{11}\hat{H}_{23}-\hat{H}_{14}\hat{H}_{33} & \hat{H}_{33}\hat{H}_{44}-\hat{H}_{14}\hat{H}_{23}-4\hat{\Omega}^2\end{bmatrix} \times\begin{bmatrix}\eta_2\\ \eta_3\end{bmatrix}=0 . \tag{45}$$

The characteristic equation of this 2×2 matrix is then

$$16\hat{\Omega}^4-4T\hat{\Omega}^2+\Delta_{14}\Delta_{23}=0 , \tag{46}$$

where we have used the substitutions

$$T=H_{11}H_{22}+H_{33}H_{44}-2H_{14}H_{23} , \tag{47a}$$

$$\Delta_{14}=\hat{H}_{11}\hat{H}_{44}-(\hat{H}_{14})^2 , \tag{47b}$$

$$\Delta_{23}=\hat{H}_{22}\hat{H}_{33}-(\hat{H}_{23})^2 . \tag{47c}$$

The squared characteristic frequencies are then given by

$$\hat{\Omega}_{\pm}^2=[T\pm(T^2-4\Delta_{14}\Delta_{23})^{1/2}]/8 , \tag{48}$$

while the positivity conditions which ensure the existence of real frequencies are

$$0\le(4\Delta_{14}\Delta_{23})^{1/2}\le T .$$

Provided these inequalities are satisfied, the squared frequencies $\hat{\Omega}_{\pm}^2$ may be determined, and one may solve for the quantities η_1, η_3, and η_4 in terms of η_2. Given the form of the equations, one may choose all the η_k to be real. It follows that if the variable A satisfies Eq. (42) with a given value of $\hat{\Omega}$, then its complex conjugate A^* satisfies it with $-\hat{\Omega}$. The normalization of the variable A is then obtained by requiring that the Poisson bracket of A with its complex conjugate A^* be the same as that of a with a^*, namely,

$$\{A,A^*\}=ik_w/mc , \tag{49}$$

which is equivalent to imposing

$$\eta_1\eta_2+\eta_3\eta_4=1 . \tag{50}$$

This normalization not only fixes the coefficients η_k (to within an overall sign), but it also determines the *sign* of the frequency $\hat{\Omega}$. Working out the details, we find that the signs of the frequencies are given by

$$\mathrm{sgn}\hat{\Omega}_+=\mathrm{sgn}(4\hat{\Omega}_+^2\hat{H}_{44}-\Delta_{14}\hat{H}_{22}) , \tag{51a}$$

$$\mathrm{sgn}\hat{\Omega}_-=\mathrm{sgn}(\Delta_{14}\hat{H}_{22}-4\hat{\Omega}_-^2\hat{H}_{44}) . \tag{51b}$$

The product of the factors on the right-hand sides is $\Delta_{14}(\hat{H}_{23}\hat{H}_{44}-\hat{H}_{41}\hat{H}_{22})^2$, which implies that the product of the frequencies $\hat{\Omega}_+\hat{\Omega}_-$ has the same sign as Δ_{14}. If $\Delta_{14}>0$, the sum of the factors is $4(\hat{\Omega}_+^2-\hat{\Omega}_-^2)\hat{H}_{44}$. It turns out that this quantity is positive whenever $\Delta_{14}>0$, and one finds that both $\hat{\Omega}_+$ and $\hat{\Omega}_-$ are positive. In contrast, if $\Delta_{14}<0$, the two frequencies necessarily are of opposite sign, and it is essential to know which one is positive. To find out we form the difference of the factors on the right-hand side of Eqs. (51). We find $4(\hat{\Omega}_+^2+\hat{\Omega}_-^2)\hat{H}_{44}-2\Delta_{14}\hat{H}_{22}$, which turns out to be positive when $\Delta_{14}<0$. It follows that the frequency $\hat{\Omega}_+$ is always positive, whereas $\hat{\Omega}_-$ has the sign of Δ_{14}. The occurrence of a negative frequency is an important aspect of our work, since it means that a fixed point, which is certainly an extremum of the Hamiltonian, is not necessarily a minimum. Only for the group-II normal fixed points are both frequencies positive, and the corresponding Hamiltonian a local minimum.

The quantities T, Δ_{14}, and Δ_{23} may be evaluated analytically. Using the formula for the matrix elements $\hat{H}_{kl}$ given in the Appendix, we find

$$\hat{\Omega}_+^2+\hat{\Omega}_-^2=T/4 =(\hat{\Omega}_0/\gamma_f)^2[r_f^2+(r_f-1)^2/(1+\hat{\rho}_f^2)] , \tag{52a}$$

$$\Delta_{23}=8(\hat{\Omega}_0\hat{\Omega}_w/\gamma_f^2)r_fI_1'(\hat{\rho}_f)/\hat{\rho}_f , \tag{52b}$$

$$\Delta_{14}=4(\hat{\Omega}_0/\gamma_f)^2r_f\hat{\rho}_f\frac{d(P_z/\hat{\Omega}_0)}{d\hat{\rho}_f} , \tag{52c}$$

where the quantity $d(P_z/\hat{\Omega}_0)/d\hat{\rho}_f$ may be written, calculating the derivative of Eq. (35), in the form

$$\frac{d(P_z/\Omega_0)}{d\hat{\rho}_f}=\hat{\rho}_f-\frac{B_w}{B_0}(1+\hat{\rho}_f^2)\frac{(2\hat{\rho}_f^2-1)I_0(\hat{\rho}_f)+3I_2(\hat{\rho}_f)}{\hat{\rho}_f^2} . \tag{53}$$

These expressions, which yield analytic results for the sum and product of the squared frequencies, agree with those derived by Freund and Ganguly in Ref. [1].

The positivity condition that $\Delta_{14}\Delta_{23} \geq 0$, given our explicit expressions, reduces simply to requiring that $d(P_z/\hat{\Omega}_0)/d\hat{\rho}_f \geq 0$. This justifies our assertion, made in the preceding section, that the extrema of the graph of P_z vs $\hat{\rho}_f$ were the limits of stable oscillations. We note also that, in the region of stability, the sign of Δ_{14} is given by the product $r_f\hat{\rho}_f$. Group-I motion has $r_f > 0$ and $\hat{\rho}_f \leq 0$, while group II has $\hat{\rho}_f \geq 0$, with $r_f \geq 0$ for normal motion and $r_f \leq 0$ for the reversed-field (antiparallel) configuration. Consequently, the frequency $\hat{\Omega}_-$ is positive for group-II normal, and negative in the other two configurations. A simple way of seeing this is to observe that the product $\Delta_{14}\Delta_{23}$ has a double zero at $r_f = 0$, which corresponds to a simple zero, or change of sign of $\hat{\Omega}_-$.

The expressions we have found show that the frequencies $\hat{\Omega}_\pm$ may be written in the form

$$\hat{\Omega}_\pm = (\hat{\Omega}_0/\gamma_f)F_\pm(\hat{\rho}_f, B_w/B_0) , \tag{54}$$

where the dimensionless functions $F_\pm$ depend only on the ratio of the wiggler to the axial field and the value of $\hat{\rho}_f$ at the fixed point. The overall normalization is then provided by the dimensionless relativistic cyclotron frequency $\hat{\Omega}_0/\gamma_f$. In Fig. 4 we show the quantities $F_\pm$ as functions of $\hat{\rho}_f$ for $B_w/B_0 = 0.1$ and in Fig. 5 for $B_w/B_0 = 0.2$. In each figure the range of $\hat{\rho}_f$ has been limited to values such that the frequency $\hat{\Omega}_-$ is real. In addition, we show also the quantity r_f defined in Eq. (37).

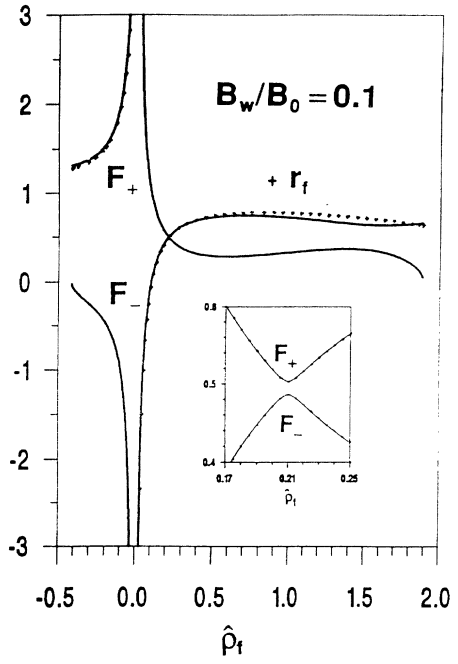

FIG. 4. The quantities $F_\pm = \gamma_f\hat{\Omega}_\pm/\hat{\Omega}_0$ as functions of $\hat{\rho}_f$ over the domain for which F_- is real, when the ratio $B_w/B_0 = 0.1$. The crosses represent the quantity $r_f = (\gamma\beta_z)_f/\hat{\Omega}_0$. The inset shows the detail of the repulsion of the frequencies.

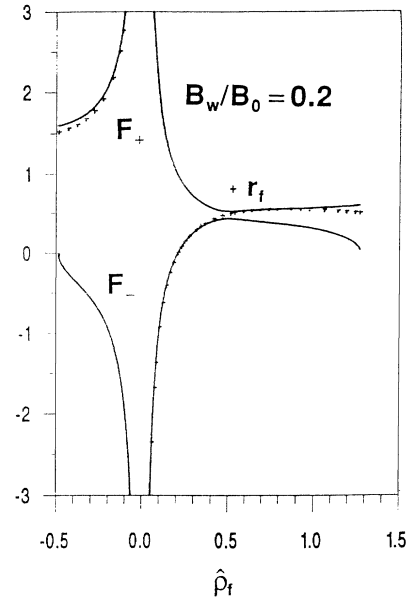

FIG. 5. Same as in Fig. 4, but with the ratio $B_w/B_0 = 0.2$. The repulsion of the frequencies is more clearly apparent.

The quantity $(r_f\hat{\Omega}_0/\gamma_f)$ is the axial velocity β_z at the fixed point. We see that in group I ($\hat{\rho}_f < 0$), the quantities r_f and F_+ are approximately equal. This implies that the frequency $\hat{\Omega}_+$ is nearly equal to $(\beta_z)_f$. Similarly for positive $\hat{\rho}_f$ (group II), we see that r_f is approximately equal to F_- for small $\hat{\rho}_f$ and roughly equal to F_+ for larger values of $\hat{\rho}_f$. Thus we find that one of the characteristic frequencies is always approximately equal to the axial velocity, although a crossover takes place when r_f has the approximate value of $\frac{1}{2}$. In Fig. 4, the inset shows how the two frequencies repel each other, a well-known phenomenon in quantum mechanics. The quantities $F_\pm$ diverge as $\hat{\rho}_f^{-1}$ for small $\hat{\rho}_f$, but this is compensated by the factor $\hat{\Omega}_0/\gamma_f$, which behaves like $|\hat{\rho}_f|$. Consequently, the frequencies $\hat{\Omega}_\pm$ approach the values ± 1 as $\hat{\rho}_f$ approaches zero.

B. The Jacobi identity and the normal modes

Given any three dynamical variables A, B, and C, the Jacobi identity for the Poisson brackets imposes

$$\{A,\{B,C\}\}+\{B,\{C,A\}\}+\{C,\{A,B\}\}=0 . \tag{55}$$

If we choose A_+, A_-, and $\hat{H}_Q$, the quadratic Hamiltonian, as the three variables, we find the relation

$$(\hat{\Omega}_+ + \hat{\Omega}_-)\{A_+, A_-\} = 0 , \tag{56}$$

which follows from the fact that the Poisson bracket $\{A_+, A_-\}$, being only a number, has itself a zero Poisson bracket with $\hat{H}_Q$. Similarly, we obtain

$$(\hat{\Omega}_+ - \hat{\Omega}_-)\{A_+, A_-^*\} = 0 . \tag{57}$$

Provided that the frequencies are different, the Poisson brackets $\{A_+, A_-\}$ and $\{A_+^*, A_-\}$ are zero, which implies that the transformation from the dynamical vari-

ables $(a-a_f)$ and $(b-ib_f)$ to A_+ and A_- is canonical. The quadratic piece of the Hamiltonian thus may be written as

$$\hat{H}_Q=\hat{\Omega}_+|A_+|^2+\hat{\Omega}_-|A_-|^2 . \tag{58}$$

The solution to Hamilton's equations are simply

$$A_\pm(\hat{t})=A_\pm(0)e^{i\hat{\Omega}_\pm\hat{t}} , \tag{59}$$

where the complex numbers $A_\pm(0)$ are the initial values of the new dynamical variables. Thus there exist two constants of motion, $|A_+(0)|$ and $|A_-(0)|$. The complete solution to the problem, in the quadratic approximation, has thus been found.

The new variables A_+ and A_- and the quantities $(a-a_f)$ and $(b-ib_f)$ are related in Eq. (43) through the quantities we called η_k. In preference to these, we use the real coefficients $C_{\pm a}$, $C_{\pm a^*}$, $C_{\pm b}$, and $C_{\pm b^*}$, which relate the old and new variables as follows:

$$A_\pm=C_{\pm a}(a-a_f)+C_{\pm a^*}(a-a_f)^* +i[C_{\pm b}(b-ib_f)+C_{\pm b^*}(b-ib_f)^*] , \tag{60a}$$

$$a-a_f=C_{+a}A_+-C_{+a^*}A_+^*+C_{-a}A_--C_{-a^*}A_-^* , \tag{60b}$$

$$b-ib_f=-i[C_{+b}A_++C_{+b^*}A_+^*+C_{-b}A_- +C_{-b^*}A_-^*] . \tag{60c}$$

Detailed formulas for these coefficients, which depend only on the ratio B_w/B_0 and $\hat{\rho}_f$, are given in the Appendix. We show the general behavior of the coefficients as functions of $\hat{\rho}_f$ in Figs. 6–13. In particular, in Fig. 6 we show the four coefficients C_{+a}, C_{+a^*}, C_{+b}, and C_{+b^*} as functions of $\hat{\rho}_f$ over the domain of negative values for which the frequency $\hat{\Omega}_-$ is real and negative (group I), with the ratio $B_w/B_0=0.1$. Figure 7 shows C_{-a}, C_{-a^*}, C_{-b}, and C_{-b^*} over the same domain, while the behavior of the coefficients for positive allowed values of $\hat{\rho}_f$ (group II) is illustrated in Figs. 8 and 9. In Figs. 10–13 we show the same quantities as in Figs. 6–9 but with the ratio $B_w/B_0=0.2$. In all figures, the coefficients

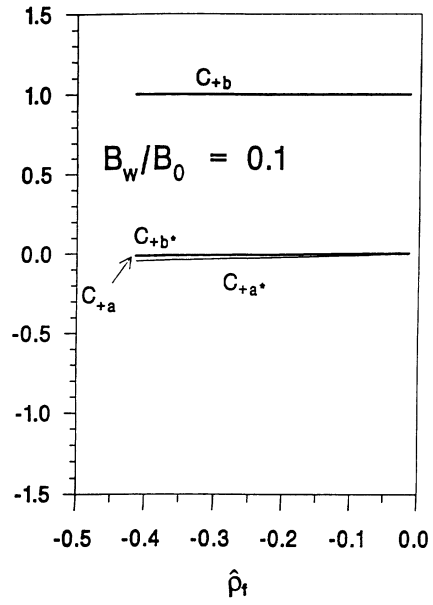

FIG. 6. The coefficients of the normal mode A_+ as functions of $\hat{\rho}_f$ in the stability region for group I, with $B_w/B_0=0.1$. C_{+a} and C_{+b} are shown as thick lines, C_{+a^*} and C_{+b^*} as thin lines.

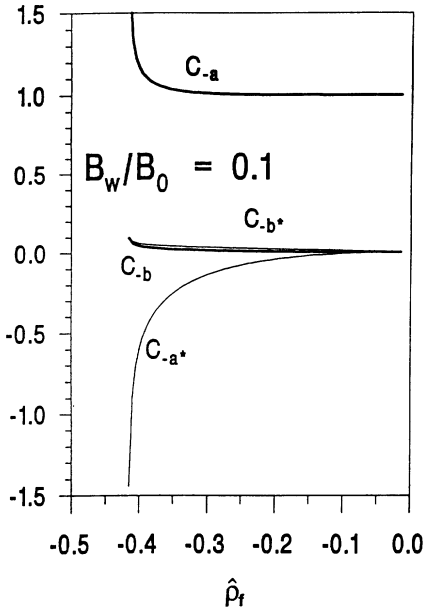

FIG. 7. The coefficients of the normal mode A_- as functions of $\hat{\rho}_f$ in the stability region for group I, with $B_w/B_0=0.1$. C_{-a} and C_{-b} are shown as thick lines, C_{-a^*} and C_{-b^*} as thin lines.

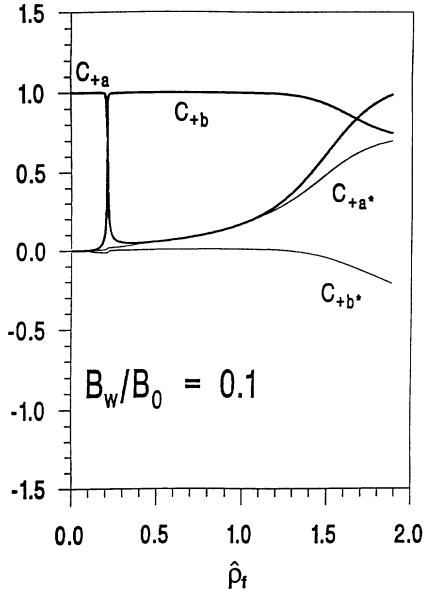

FIG. 8. The coefficients of the normal mode A_+ as functions of $\hat{\rho}_f$ in the stability region for group II, with $B_w/B_0=0.1$.

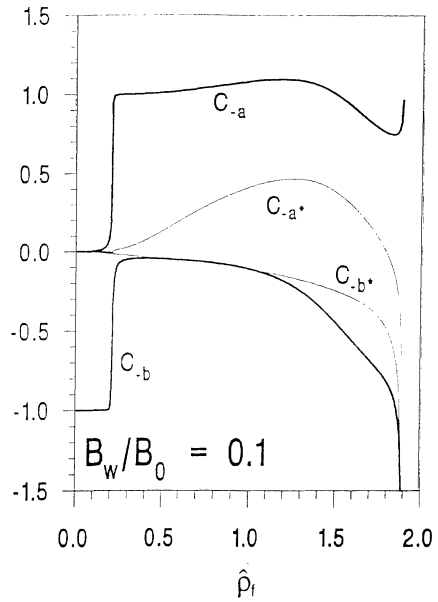

FIG. 9. The coefficients of the normal mode A_- as functions of $\hat{\rho}_f$ in the stability region for group II, with $B_w/B_0=0.1$.

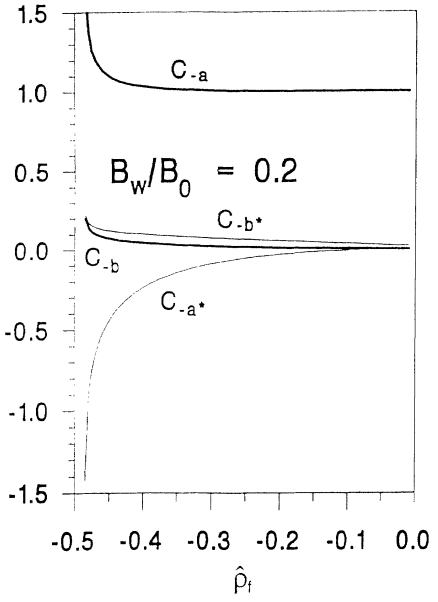

FIG. 11. The coefficients of the normal mode A_- as functions of $\hat{\rho}_f$ in the stability region for group I, with $B_w/B_0=0.2$.

C_{+a}, C_{+b}, C_{-a}, and C_{-b} are represented by thick lines, while the coefficients C_{+a*}, C_{+b*}, C_{-a*}, and C_{-b*} are shown as thin lines.

The behavior of the coefficients as functions of $\hat{\rho}_f$ is one of the most important aspects of our work, and we describe the key features in some detail. First we see in both Figs. 6 and 10 that for group I the coefficient $C_{+b}\approx 1$, while C_{+a}, C_{+b*}, and C_{+a*} are much smaller in magnitude. This implies that the variable A_+ is quasi-identical with $(ib+b_f)$. One then expects that the variable A_- should mainly involve $(a-a_f)$ and $(a-a_f)^*$. Inspection of Figs. 7 and 11 shows that the coefficients C_{-b} and C_{b*} are indeed small, while near the stability limits (where the frequency $\hat{\Omega}_-$ becomes imaginary), both coefficients C_{-a} and C_{-a*} diverge. This divergence is accompanied by a vanishing of the frequency, so that the quadratic Hamiltonian remains finite. For smaller values of $|\hat{\rho}_f|$, we observe that $C_{-a}\approx 1$ with $C_{-a*}\approx 0$, which means that $A_-\approx(a-a_f)$. This favor-

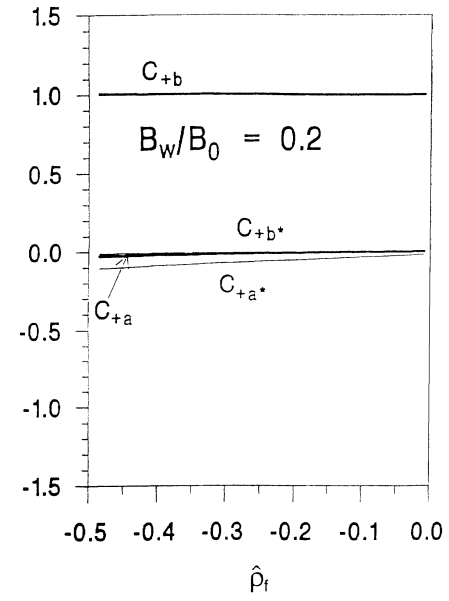

FIG. 10. The coefficients of the normal mode A_+ as functions of $\hat{\rho}_f$ in the stability region for group I, with $B_w/B_0=0.2$.

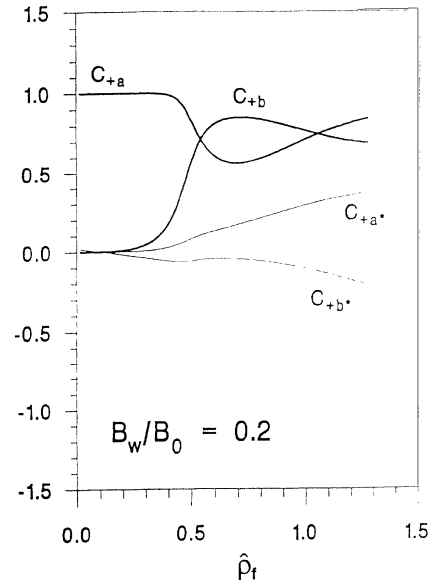

FIG. 12. The coefficients of the normal mode A_+ as functions of $\hat{\rho}_f$ in the stability region for group II, with $B_w/B_0=0.2$.

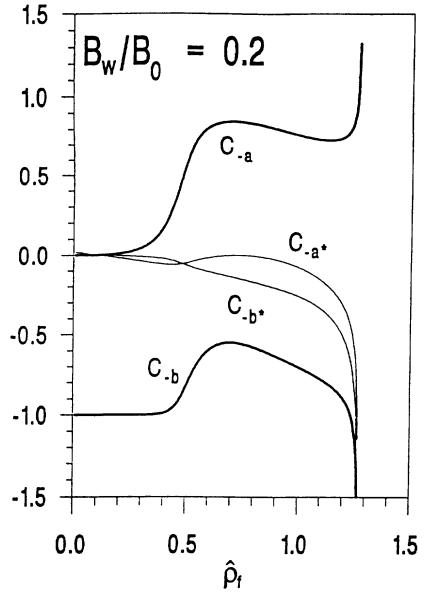

FIG. 13. The coefficients of the normal mode A_- as functions of $\hat{\rho}_f$ in the stability region for group II, with $B_w/B_0=0.2$.

able situation is obtained, however, only for relatively large values of the ratio $P_z/\hat{\Omega}_0$, which requires either high energy or small axial fields. The admixture of $(a-a_f)^*$ increases with increasing $|\hat{\rho}_f|$, making the trajectory of the variable a elliptic rather than circular. Quasicircular motion is preferable, since the axial velocity has less ripple. On the basis of these figures, we infer that group-I motion presents no particular difficulties, provided a safety margin from the stability limit is maintained.

The situation for group-II motion is much more complex, as is apparent in Figs. 8, 9, 12, and 13. First we note that, in the reversed-field configuration, with beam and axial fields antiparallel, and which is characterized by small positive values of $\hat{\rho}_f$ ($<B_w/B_0$), the behavior is exceedingly simple. The coefficients C_{+a} and C_{-b} are very close to 1 and -1, respectively, and all others are quite small. The variable A_+ may thus be identified with $(a-a_f)$, while A_- is quite accurately $(-ib-b_f)$. The trajectories of the variables a and b in the complex plane are thus circles centered at a_f and ib_f, swept out with frequencies $\hat{\Omega}_+$ and $\hat{\Omega}_-$, respectively [here $(\beta_z)_f$ is negative and roughly equal to the frequency $\hat{\Omega}_-$]. The situation is quite similar to the one-dimensional treatment, for which the quantity $be^{-i\hat{z}}$ is a constant of the motion. We thus expect the trajectories in the reversed-field mode to be quite well behaved. However, two important caveats concern the neighborhood of the antiresonance, where $r_f=-1$. First, the ratio of the frequencies there is approximately -2, which may lead to "small-denominator" effects, particularly in the cubic terms we neglect. The second is discussed below, where the trajectories in the Cartesian coordinate variables are examined.

This simple and favorable situation persists into the normal group-II region $[(\beta_z)_f>0]$ up to the value of $\hat{\rho}_f$ where the frequencies repel each other (this happens when $r_f\approx 0.5$). It is clear in Figs. 8 and 9 that an extremely brusque exchange of roles between a and b takes place. In a small interval in $\hat{\rho}_f$, near $\hat{\rho}_f=0.21$, the magnitudes of the coefficient C_{+a} and C_{-b} plunge rapidly by an order of magnitude while C_{+b} and C_{-a} rise from ≈ 0 to ≈ 1. This corresponds to the well-known phenomenon in quantum mechanics where the repulsion of energy levels is accompanied by exchange of the wave functions. Here this means that for $\hat{\rho}_f<0.19$, the variable $(b-ib_f)$ traces out a circle at frequency $\hat{\Omega}_-\approx(\beta_z)_f$, while for $\hat{\rho}_f>0.23$ (but not too much greater), it traces out a circle at frequency $\hat{\Omega}_+$ which is again $\approx(\beta_z)_f$. Thus on either side of the transition one finds that $(b-ib_f)e^{-i\hat{z}}$ is an approximate constant of the motion, just as in the 1D case. The variable a does essentially the opposite, but for $\hat{\rho}_f>0.5$ we observe in Fig. 9 that C_{-a^*} becomes nonnegligible, which will lead to complicated trajectories. At still larger $\hat{\rho}_f$, all coefficients become significant, and the simple behavior of the amplitudes A_+ and A_- is no longer reflected in the trajectories of the variables a and b. Near the limits of stability the divergence of the coefficients C_- is again apparent in Fig. 9.

For the larger value of $B_w/B_0=0.2$, the transition region, as may be seen in Figs. 12 and 13, is much broader in the variable $\hat{\rho}_f$, and the transition itself is not complete. The coefficients C_{-b} and C_{+a} do not fall to ≈ 0, nor do C_{-a} and C_{+b} rise to ≈ 1. This means that for no values of $\hat{\rho}_f>0.4$ may one expect simple trajectories for the variables a and b. This tendency obviously worsens with increasing B_w/B_0. We thus conclude that the successful operation of a FEL at values of $\hat{\rho}_f\approx 1$, although allowed in principle, is probably unlikely.

C. Calculation of the orbits

The explicit calculation of the motion of an electron for which the quadratic approximation to the Hamiltonian is adequate proceeds as follows. The initial data may be taken to consist of the Cartesian position and velocity coordinates at the instant $t=0$. Following the chain of canonical transformations presented in Sec. II, one computes the initial values of the dynamical variables a and b together with the value of the conserved quantity P_z. Provided that the values of the ratios $P_z/\hat{\Omega}_0$ and B_w/B_0 are such that a stable fixed point exists, one may then calculate the relevant associated quantities $\hat{\rho}_f$, a_f, b_f, γ_f, $(\beta_z)_f$, the characteristic frequencies $\hat{\Omega}_\pm$, and the coefficients C_{+a}, etc. From the initial values of a and b, using a_f, b_f, and the coefficients C_{+a}, the initial values of the harmonic oscillator amplitudes $A_\pm$ may be determined. We write them in the form

$$A_\pm(0)=|A_\pm|e^{i\psi_\pm}\ , \tag{61}$$

where the magnitudes $|A_\pm|$ are constants of the motion and $\psi_\pm$ are the initial phases. In this way we obtain six independent initial values, $|A_\pm|$, $\psi_\pm$, P_z, and $\hat{z}(0)$, from the six initial position and velocity coordinates. At this point, one should compare the numerical value of the energy γ, as computed directly from the initial velocities,

with the corresponding value for the quadratic Hamiltonian, $\gamma_f+\hat{\Omega}_+|A_+|^2+\hat{\Omega}_-|A_-|^2$. Our experience is that when these numbers differ by $<0.1\%$, our simulated trajectories agree closely with those calculated numerically. Although the time evolution of the variables $A_\pm$ is quite simple, the consequences for the orbital motion of the electron can be quite complicated, as we shall now show.

In order to find the instantaneous position of the electron, it is first necessary to compute its axial position $\hat{z}(\hat{t})$. By inserting into Eq. (25) the explicit time dependence of the variables a and b, and neglecting terms of order higher than quadratic in the amplitudes $|A_\pm|$, we find $\beta_z(\hat{t})$, which is given by

$$\frac{d\hat{z}}{d\hat{t}}(\hat{t})=(\beta_z)_f+\delta\beta_z+E_1\cos(\hat{\Omega}_+\hat{t}+\psi_+)+E_2\cos(\hat{\Omega}_-\hat{t}+\psi_-)+E_3\cos[2(\hat{\Omega}_+\hat{t}+\psi_+)]$$
$$+E_4\cos[2(\hat{\Omega}_-\hat{t}+\psi_-)]+E_5\cos[(\hat{\Omega}_++\hat{\Omega}_-)\hat{t}+\psi_++\psi_-]+E_6\cos[(\hat{\Omega}_+-\hat{\Omega}_-)\hat{t}+\psi_+-\psi_-]\ . \tag{62}$$

In this expression, $(\beta_z)_f$ is the value at the fixed point, and the quantities $\delta\beta_z$ and E_k may be written as follows:

$$\delta\beta_z=[|A_+|^2(C_{+b}^2+C_{+b^*}^2-C_{+a}^2-C_{+a^*}^2-(\beta_z)_f\hat{\Omega}_+)+|A_-|^2(C_{-b}^2+C_{-b^*}^2-C_{-a}^2-C_{-a^*}^2-(\beta_z)_f\hat{\Omega}_-)]/\gamma_f\ , \tag{63a}$$

$$E_1=-2|A_+|[a_f(C_{+a}-C_{+a^*})+b_f(C_{+b}+C_{+b^*})]/\gamma_f\ , \tag{63b}$$

$$E_2=-2|A_-|[a_f(C_{-a}-C_{-a^*})+b_f(C_{-b}+C_{-b^*})]/\gamma_f\ , \tag{63c}$$

$$E_3=2|A_+|^2(C_{+a}C_{+a^*}+C_{+b}C_{+b^*})/\gamma_f\ , \tag{63d}$$

$$E_4=2|A_-|^2(C_{-a}C_{-a^*}+C_{-b}C_{-b^*})/\gamma_f\ , \tag{63e}$$

$$E_5=2|A_+A_-|(C_{+b}C_{-b}+C_{+b^*}C_{-b^*}-C_{+a}C_{-a}-C_{+a^*}C_{-a^*})/\gamma_f\ , \tag{63f}$$

$$E_6=2|A_+A_-|(C_{+b}C_{-b^*}+C_{+b^*}C_{-b}+C_{-a}C_{-a^*}+C_{+a^*}C_{-a})/\gamma_f\ . \tag{63g}$$

We thus see that the axial velocity is perturbed from its ideal fixed-point value $(\beta_z)_f$ by a time-independent correction $\delta\beta_z$ which is quadratic in the amplitudes $|A_\pm|$, as well as six oscillatory terms, of which two are linear in $|A_\pm|$ and have the characteristic frequencies $\hat{\Omega}_\pm$, and four others which are quadratic in $|A_\pm|$, and which oscillate at the sum and difference frequencies. These ripple effects in the longitudinal velocity can give rise to emission of radiation at sidebands of the principal frequency. Subsequent integration yields the axial position as a function of time,

$$\hat{z}(\hat{t})=\hat{z}(0)+[(\beta_z)_f+\delta\beta_z]\hat{t}+(E_1/\hat{\Omega}_+)[\sin(\hat{\Omega}_+\hat{t}+\psi_+)-\sin\psi_+]+(E_2/\hat{\Omega}_-)[\sin(\hat{\Omega}_-\hat{t}+\psi_-)-\sin\psi_-]$$
$$+[E_3/(2\hat{\Omega}_+)]\{\sin[2(\hat{\Omega}_+\hat{t}+\psi_+)]-\sin2\psi_+\}+[E_4/(2\hat{\Omega}_-)]\{\sin[2(\hat{\Omega}_-\hat{t}+\psi_-)]-\sin2\psi_-\}$$
$$+[E_5/(\hat{\Omega}_++\hat{\Omega}_-)]\{\sin[(\hat{\Omega}_++\hat{\Omega}_-)\hat{t}+\psi_++\psi_-]-\sin(\psi_++\psi_-)\}$$
$$+[E_6/(\hat{\Omega}_+-\hat{\Omega}_-)]\{\sin[(\hat{\Omega}_+-\hat{\Omega}_-)\hat{t}+\psi_+-\psi_-]-\sin(\psi_+-\psi_-)\}\ . \tag{64}$$

This expression shows that if any of the three quantities $\hat{\Omega}_-$, $\hat{\Omega}_+\pm\hat{\Omega}_-$ are very small, the deviation from the ideal position coordinate may become appreciable even if the amplitudes $|A_\pm|$ are acceptably small. Consequently, the operating conditions should be chosen so as to avoid this difficulty. Since $\hat{\Omega}_-$ vanishes at the limits of stability, it is clear that operation too close to the limits is likely to be unsuccessful. The difference $\hat{\Omega}_+-\hat{\Omega}_-$ becomes small in the region where the frequencies attempt to cross, hence this is also an unsuitable operating region.

Once the longitudinal coordinate $\hat{z}(\hat{t})$ has been computed, Eq. (18a) provides us with an explicit expression for the transverse position

$$\hat{x}(\hat{t})+i\hat{y}(\hat{t})=\hat{\rho}_f e^{i\hat{z}(\hat{t})}+(2/\hat{\Omega}_0)^{1/2}[(C_{+a}-C_{+b^*})A_+-(C_{+a^*}+C_{+b})A_+^*$$
$$+(C_{-a}-C_{-b^*})A_--(C_{-a^*}+C_{-b})A_-^*]e^{i\hat{z}(\hat{t})}\ , \tag{65}$$

where by $A_\pm$ we mean the time-dependent values $|A_\pm|e^{i(\psi_\pm+\hat{\Omega}_\pm\hat{t})}$. We observe that the transverse motion consists of a linear superposition of five circular motions, one that corresponds to the ideal axially centered helical motion of scaled radius $\hat{\rho}_f$, and four that are linear in the oscillator amplitudes. The phase of the principal circular motion is $\hat{z}(\hat{t})$, while the four parasitic amplitudes have phases $\hat{z}(\hat{t})\pm(\psi_\pm+\hat{\Omega}_\pm\hat{t})$. Since $\hat{z}(\hat{t})$ has oscillatory pieces in addition to the term linear in time, the true time dependence of $\hat{x}+i\hat{y}$ is quite complex, and the Fourier spectrum involves several frequencies.

The transverse velocity of the electron may be evaluated in two different ways. One is simply to compute the time

derivative of the transverse position coordinate, which yields the following expression:

$$\beta_x(\hat{t})+i\beta_y(\hat{t})=ie^{i\hat{\varphi}(\hat{t})}(\beta_z(\hat{t})\hat{\rho}_f+(2/\hat{\Omega}_0)^{1/2}\{[\beta_z(\hat{t})+\hat{\Omega}_+](C_{+a}-C_{-b}^*)A_+-[\beta_z(\hat{t})-\hat{\Omega}_+](C_{+a}^*+C_{+b})A_+^* +[\beta_z(\hat{t})+\hat{\Omega}_-](C_{-a}-C_{-b}^*)A_--[\beta_z(\hat{t})-\hat{\Omega}_-](C_{-a}^*+C_{-b})A_-^*\}) , \tag{66}$$

where again the time-dependent $A_\pm$ are understood. In this expression, the time-dependent pieces of $\beta_z(\hat{t})$, which are of first and second order in the amplitudes $|A_\pm|$, induce an even more complex time dependence. However, one may also use Eqs. (12b) and (22), which through Hamilton's equations, yields directly

$$\beta_x(\hat{t})+i\beta_y(\hat{t})=ie^{i\hat{\varphi}(\hat{t})}[(2\hat{\Omega}_0)^{1/2}a-\hat{\Omega}_w J]/\gamma , \tag{67}$$

where the expression on the right-hand side is to be evaluated by expanding the complex quantity J about the fixed point. The result of doing so agrees with the preceding expression for the transverse velocity in terms which are of zero and first orders in the amplitudes $|A_\pm|$, but not at the level of quadratic terms. This is a regrettable but unavoidable consequence of our quadratic approximation to the Hamiltonian. Our neglect of cubic terms in the Hamiltonian means that our velocities are not consistent at the quadratic approximation. In principle, if the amplitudes are small, the discrepancy between our two transverse velocities is not significant. However, there is a possibility that in the expansion of the right-hand side of Eq. (67) a second-order term may appear with an extremely weak time dependence, essentially the difference of two nearby frequencies. Such a term produces a slow transverse drift, which could lead to some electrons entering into collision with the transverse confining structure. Our calculation of the transverse position via Eq. (65) does not allow for such a possibility, but it remains a potential difficulty, especially when frequency differences are extremely small.

The behavior of the position and velocities as a function of time, even when our quadratic approximation is valid, is rather complicated. We have compared our results with numerical calculation of the trajectories in the various regimes, and we find that our description is quite good when the oscillator amplitudes are of magnitude 0.1. In a large number of situations we found that fair quantitative agreement could be obtained with a simplified approach, which we outline below.

V. SIMPLE APPROXIMATE DESCRIPTION OF TRAJECTORIES

The preceding treatment has considered in great detail the most general motion which our model can predict. In this section we present a simplified approximate description of the trajectories. We obtain this by setting equal to zero a certain number of quantities which are numerically quite small over a certain domain of parameters. What emerges, at least in the favorable situations, is a quantitatively correct but quite simple description of the trajectories in terms of the ideal helical motion accompanied by a very slow rotation of the instantaneous center of gyration as well as a parasitic cyclotronic motion. The axial velocity of an electron oscillates about its ideal value at a single frequency, giving rise to a fairly simple Fourier spectrum for the transverse motion. Consequently, the calculation of the spontaneous emission spectrum is relatively simple compared to the general case. In the Appendix this spectrum is calculated for the case of free space, assuming only one axial velocity ripple frequency and one cyclotronic transverse motion.

Although the motion we predict in general may be quite complex, inspection of our Figs. 6–13 shows that for certain ranges of the scaled radius $|\hat{\rho}_f|$, all but two of the coefficients $C_{\pm a}$, etc., are quite small. Next, we note that in general $b_f \ll a_f$, and it might be reasonable to neglect it. If we also take into account the fact that one of the frequencies $\hat{\Omega}_\pm$ is almost equal to the axial velocity at the fixed point, we obtain a greatly simplified description of the motion. In fact, we find two distinct simplified descriptions, depending on whether the quantity $\gamma_f(\beta_z)_f/\hat{\Omega}_0$ is $>\frac{1}{2}$ or $<\frac{1}{2}$. In what follows we discuss in detail these two situations. It must be noted that when we write equations, they should be interpreted as valid only to the neglect of certain small quantities, and not as exact expressions.

If $\gamma_f(\beta_z)_f/\hat{\Omega}_0>\frac{1}{2}$ [but largely excluding the unstable band near $\gamma_f(\beta_z)_f/\hat{\Omega}_0=1$], we may use

$$\hat{\Omega}_+\approx(\beta_z)_f, \quad C_{-a}=1, \quad C_{+b}=1 ,$$

and all others zero. For the shift in mean longitudinal velocity we find

$$\delta\beta_z=\{|A_+|^2[1-(\beta_z)_f\hat{\Omega}_+] +|A_-|^2[1-(\beta_z)_f\hat{\Omega}_-]\}/\gamma_f , \tag{68}$$

which implies that increasing the oscillator amplitude A_+ produces a small increase in speed, while increasing A_- has the opposite effect.

All the quantities E_k are zero except

$$E_2=-2|A_-|a_f/\gamma_f , \tag{69}$$

which implies that the ripple in longitudinal speed is caused mainly by the A_- amplitude, and has the frequency $\hat{\Omega}_-$. The transverse position is then given by

$$\hat{x}(\hat{t})+i\hat{y}(\hat{t})=\hat{\rho}_f e^{i\hat{\varphi}(\hat{t})}+(2/\hat{\Omega}_0)^{1/2}[-A_+^*+A_-]e^{i\hat{\varphi}(\hat{t})} , \tag{70}$$

which corresponds to a superposition of three circular motions, one of which is the projected ideal helical motion of scaled radius $|\hat{\rho}_f|$, while the other two have

scaled radii of $(2/\hat{\Omega}_0)^{1/2}|A_+|$ and $(2/\hat{\Omega}_0)^{1/2}|A|$, respectively. If we neglect the ripple and shift of β_z, then the three circles are swept out uniformly in time at the respective frequencies $(\beta_z)_f$, $(\beta_z)_f-\hat{\Omega}_+$, and $(\beta_z)_f+\hat{\Omega}_-$. Taking into account the near equality of $(\beta_z)_f$ and $\hat{\Omega}_+$, we see that the amplitude A_+ corresponds to an extremely slow rotation. This has been described in the literature as the guide center motion, about which the more rapid circular motions occur. The radius of the circle described by the guide center is determined by $|A_+|$, which is essentially the modulus of the initial value of our dynamical variable $b-ib_f$. The desired FEL motion then occurs about this displaced guide center, and is accompanied by the additional circular motion at the frequency $(\beta_z)_f+\hat{\Omega}_-$. If one excludes the regions near the limits of stability, this frequency is to within a few percent of the relativistic cyclotron frequency $\hat{\Omega}_0/\gamma_f$. The radius of this cyclotronic motion is thus determined by $|A_-|$, which is essentially given by the modulus of the initial value of $(a-a_f)$. Thus our simple description leads to an interpretation of the transverse motion as a superposition of three circular movements: first the ideal helical motion; second, a very slow motion of the guide center; and third, a cyclotron motion, this being also the cause of the ripple in the longitudinal velocity. This description applies to both group I and that part of group II above the transition region, the only difference being that $\hat{\Omega}_-$ is negative in the former and positive in the latter.

If $\gamma_f(\beta_z)_f/\hat{\Omega}_0<\frac{1}{2}$, which occurs typically for small positive values of $\hat{\rho}_f$, we have

$$\hat{\Omega}_-\approx(\beta_z)_f,\quad C_{+a}=1,\quad C_{-b}=-1\ ,$$

and all others zero. Now the shift in mean longitudinal velocity is given by

$$\delta\beta_z=\{|A_+|^2[-1-(\beta_z)_f\hat{\Omega}_+] -|A_-|^2[1+(\beta_z)_f\hat{\Omega}_-]\}/\gamma_f\ , \tag{71}$$

which shows that the oscillator amplitude A_- always contributes a positive shift, whereas the contribution of the amplitude A_+ produces a negative shift when $(\beta_z)_f>0$, but can have either sign when $(\beta_z)_f<0$. The effect on the mean longitudinal speed of increasing $|A_-|$ is thus an increase in normal group-II operation and a decrease in the antiparallel configuration. Increasing $|A_+|$ always reduces mean speed in normal group-II operation. In the reversed-field configuration an increase in $|A_+|$ reduces the mean speed if the quantity $(\beta_z)_f\hat{\Omega}_+\le-1$ and increases it otherwise.

All E_k are zero except

$$E_1=-2|A_+|a_f/\gamma_f\ , \tag{72}$$

which means that the ripple in β_z is caused mainly by the A_+ amplitude, and has the frequency $\hat{\Omega}_+$. The transverse position is given by

$$\hat{x}(\hat{t})+i\hat{y}(\hat{t})=\hat{\rho}_f e^{i\hat{z}(\hat{t})}+(2/\hat{\Omega}_0)^{1/2}[A_++A_-^*]e^{i\hat{z}(\hat{t})}\ , \tag{73}$$

which again corresponds to a superposition of three circular motions, just as in the previous case. If we again neglect the ripple and shift of β_z, then the three circles are traced out at the respective frequencies $(\beta_z)_f$, $(\beta_z)_f+\hat{\Omega}_+$, and $(\beta_z)_f-\hat{\Omega}_-$. Taking into account the near equality of $(\beta_z)_f$ and $\hat{\Omega}_-$, we see that now the amplitude A_- corresponds to the slow rotation of the guide center. Here $|A_-|$ is essentially the modulus of the initial value of our dynamical variable $b-ib_f$. To a good approximation, the frequency $(\beta_z)_f+\hat{\Omega}_+$ is equal to the relativistic cyclotron frequency. The radius of the cyclotronic motion is now determined by $|A_+|$, which is again given by the modulus of the initial value of $(a-a_f)$. We thus find essentially the same description as in the previous case, except that here $(\beta_z)_f$ can be negative. The validity of this description, which applies to group-II motion below the transition region, is somewhat greater than in the preceding case, since here the stability limits are not approached. However, the helical orbits have rather small radii, which means that the transverse motion caused by the parasitic cyclotron and guide center amplitudes may be of the same order of magnitude as the desirable FEL motion.

In particular, if the operating conditions in the reversed-field configuration were chosen such that $\hat{\Omega}_+=-2(\beta_z)_f$, then the cyclotronic and ideal helical motions would have the same frequency but opposite senses—one clockwise, the other anticlockwise. When this occurs, the transverse motion of the electrons does not at all resemble our Ptolemaic picture of epicycles, but looks rather like Lissajous figures. To complicate things still further, this also corresponds to a $2:(-1)$ ratio for the frequencies $\hat{\Omega}_+$ and $\hat{\Omega}_-$. This implies that neglected cubic terms of the form $A_+A_-^2$ will be constant in time and may cause the moduli of the amplitudes $|A_+|$ and $|A_-|$ to vary with time, which would destroy our simple picture. It is interesting to note that Conde and Bekefi [4] have observed a significant loss of gain in this region. A possible explanation might be related to the fact that a given electron can exchange energy with a linearly polarized beam in both of the circular polarizations. The necessary bunching required for Madey's theorem to apply may be prevented from occurring by the interference from the opposite chirality, although detailed calculation would be required to verify this conjecture.

In the transition region, where $\gamma_f(\beta_z)_f/\hat{\Omega}_0\approx\frac{1}{2}$, and near the limits of stability, where $\hat{\Omega}_-$ vanishes, this simple approach is not even approximately valid. Indeed, inspection of Figs. 8, 9, 12, and 13 shows that in these regions our simplifying approximations are wholly inadequate. Under these circumstances the full complexity of our general treatment is needed to describe the trajectories. Even in the group-II region between the transition and the stability limit, one observes in Fig. 9 a rather significant increase of the coefficient C_{-a^*}. This is sufficient to strongly perturb our simple picture, since the ripple in axial speed becomes more complex, while an additional circular motion complicates the transverse motion. Furthermore, the rough equality between $(\beta_z)_f$ and $\hat{\Omega}_+$ weakens in this region, which means that the guide center motion becomes more rapid.

VI. CONCLUSIONS

In this work we have presented a detailed analysis of the motion of electrons in the magnetic field of a helical wiggler together with a uniform axial guide field. The principal feature of our approach is the recognition that an arbitrary trajectory is characterized by the two conserved quantities, one being the energy and the other a combination of angular and linear momentum, which we call P_z. It is the latter quantity that plays the primordial role in determining the electron's trajectory. Although the existence of this second conservation law has been known for some time, our analysis uses it to associate an ideal helical trajectory with an arbitrary trajectory. The value of P_z, as determined by the initial conditions, enables us to compute the fixed point, as well as the frequencies and coefficients of the normal modes for our two oscillators. The remaining initial conditions provide the conserved magnitudes and initial phases of the oscillators, and the analytic approximation to the true orbit may be computed. Since the initial energy is not used explicitly in calculating the oscillator amplitudes, a check of the consistency of our approach is provided by a comparison of the true energy with the sum of the fixed-point and oscillator energies. When the two agree closely, numerically calculated orbits agree quite well with those computed using our procedure.

Various pathological aspects of the orbits that have been encountered in numerical investigations may be elucidated using our approach. For some values of P_z, no fixed points exist, while for others there are two distinct stable fixed points. As the limits of stability are approached, where one of our oscillator frequencies vanish, certain normal-mode coefficients become large, and the corresponding movement erratic. Very small values of the frequency imply that the spontaneous radiation spectrum, given in the Appendix, will become extremely complex, with a large number of closely spaced peaks. Yet another difficulty occurs in the group-II mode of operation, where it may happen that our two oscillator frequencies are approximately equal. Under these circumstances, the simple picture of the transverse motion as a superposition of the ideal helical motion and the parasitic cyclotron motion is invalid. This occurs whenever $\gamma v_z = \Omega_0/2k_w$, and the FEL must be operated so as to avoid this condition. Finally, the existence of negative frequencies in the group-I and reversed-field modes of operation is a new result, which is rather surprising. Concretely it means that differences between the true energy and the energy of the ideal helical orbit can have either sign. An electron might have precisely the energy corresponding to the fixed point (which is determined by P_z) and still have appreciable oscillator amplitudes.

The limitation to small oscillator amplitudes is an unavoidable part of our treatment. There is one situation, namely, when the two oscillator frequencies are in the ratio $\pm 2{:}1$, where we expect our approach to break down, even for small amplitudes. Since the frequencies are readily calculated, it is straightforward to identify these problematic operating conditions. Finally, we remark that since the ideal helical orbit is determined by the conserved quantity P_z, it is essential that a beam of electrons, which necessarily has finite emittance, have as small dispersion in P_z as possible. In contrast to the electron's energy, which is conserved in any static magnetic field, P_z varies when the electron passes through magnetic fields which do not have the ideal screw-displacement symmetry. The effect of an adiabatic wiggler entry on the dispersion of P_z for an electron beam should therefore be an essential part of the design of an experiment.

ACKNOWLEDGMENTS

The authors would like to thank Professor G. Bekefi and Dr. C. Chen for comments on the manuscript. We have benefitted from numerous discussions with Dr. D. Gogny, Dr. J. Gardelle, Dr. J. Labrouche, and Dr. P. Le Taillandier. J.L.R. thanks Professor R. J. Temkin and Dr. B. Danly for their kind hospitality at the Plasma Fusion Center of the Massachusetts Institute of Technology, where some of this work was performed. The Laboratoire de Physique Théorique is Unité de Recherche Associée No. 764 of the Centre National de la Recherche Scientifique.

APPENDIX

Elements of the quadratic Hamiltonian $\hat{H}_Q$

The matrix elements $\hat{H}_{kl}$ may be written in the form

$$\hat{H}_{kl} = (\hat{\Omega}_0/\gamma_f)[\alpha_{kl} + \beta_{kl}(B_w/B_0) + \gamma_{kl}(B_w/B_0)^2] , \quad \text{(A1)}$$

where the coefficients α_{kl}, β_{kl}, and γ_{kl} are functions only of $\hat{\rho}_f$. The α_{kl} are given by

$$\begin{aligned} &\alpha_{11} = 2\hat{\rho}_f^2 , \\ &\alpha_{44} = \alpha_{33} = 2 , \\ &\alpha_{22} = \alpha_{14} = \alpha_{23} = 0 . \end{aligned} \quad \text{(A2)}$$

In the following expressions for β_{kl}, and γ_{kl}, the argument of the modified Bessel functions I_1 and I_3 is understood to be $\hat{\rho}_f$. We find

$$\begin{aligned} \beta_{11} &= (4\hat{\rho}_f^{-2} - 5 - 7\hat{\rho}_f^2) I_1 + (1 - \hat{\rho}_f^2) I_3 , \\ \beta_{44} &= -(4\hat{\rho}_f^{-2} + 7 + \hat{\rho}_f^2) I_1 + (3 + \hat{\rho}_f^2) I_3 , \\ \beta_{14} &= -(6 + 4\hat{\rho}_f^2) I_1 + 2 I_3 , \\ \beta_{22} &= (4\hat{\rho}_f^{-2} + 1) I_1 - I_3 , \\ \beta_{33} &= -(4\hat{\rho}_f^{-2} + 5) I_1 - 3 I_3 , \\ \beta_{23} &= -2 I_1 - 2 I_3 , \end{aligned} \quad \text{(A3)}$$

and

$$\begin{aligned} \gamma_{11} = \gamma_{44} = \gamma_{14} &= (1 + \hat{\rho}_f^2)[(13 + 12\hat{\rho}_f^{-2})(I_1)^2 \\ &\quad + (2 - 12\hat{\rho}_f^{-2}) I_1 I_3 + (I_3)^2]/2 , \end{aligned} \quad \text{(A4)}$$

$$\begin{aligned} \gamma_{22} = \gamma_{33} = \gamma_{23} &= [(5 + 4\hat{\rho}_f^{-2})(I_1)^2 + (10 + 12\hat{\rho}_f^{-2}) I_1 I_3 \\ &\quad + (I_3)^2]/2 . \end{aligned}$$

Using these expressions, one may verify that

$$\hat{H}_{11}+\hat{H}_{44}-2\hat{H}_{14}=2(\hat{\Omega}_0/\gamma_f)(1+\hat{\rho}_f^2)\ ,$$
$$\hat{H}_{22}+\hat{H}_{33}-2\hat{H}_{23}=2\hat{\Omega}_0/\gamma_f\ , \tag{A5}$$

from which it follows that the characteristic frequencies $\hat{\Omega}_+$ and $\hat{\Omega}_-$ cannot both be negative.

Expansion of the amplitudes $A_\pm$ in terms of $a-a_f$ and $b-ib_f$

In Eq. (43) we have written the amplitudes $A_\pm$ as

$$A_\pm=\eta_{\pm1}\xi^1+i(\eta_{\pm2}\xi^2+\eta_{\pm3}\xi^3)-\eta_{\pm4}\xi^4\ . \tag{A6}$$

It is more convenient to use the expression

$$A_\pm=C_{\pm a}(a-a_f)+C_{\pm a*}(a-a_f)^* +i[C_{\pm b}(b-ib_f)+C_{\pm b*}(b-ib_f)^*]\ , \tag{A7}$$

where the real coefficients C are related to η as follows:

$$C_{\pm a}=(\eta_{\pm1}+\eta_{\pm2})/2\ ,$$
$$C_{\pm a*}=(\eta_{\pm1}-\eta_{\pm2})/2\ ,$$
$$C_{\pm b}=(\eta_{\pm3}+\eta_{\pm4})/2\ ,$$
$$C_{\pm b*}=(\eta_{\pm3}-\eta_{\pm4})/2\ . \tag{A8}$$

Conversely, one may write $a-a_f$ and $b-ib_f$ in terms of $A_\pm$ and $A_\pm^*$,

$$a-a_f=C_{+a}A_+-C_{+a*}A_+^*+C_{-a}A_--C_{-a*}A_-^*\ , \tag{A9}$$

$$b-ib_f=-i[C_{+b}A_++C_{+b*}A_+^*+C_{-b}A_- +C_{-b*}A_-^*]\ . \tag{A10}$$

In contrast to the frequencies, which depend on B_0, B_w, and $\hat{\rho}_f$, the coefficients C depend only on $\hat{\rho}_f$ and the ratio B_0/B_w. Explicit expressions for them follow, which take different forms, depending on the signs of the two quantities

$$R=\hat{H}_{11}\hat{H}_{23}-\hat{H}_{33}\hat{H}_{14} \tag{A11}$$

and

$$S=\hat{H}_{44}\hat{H}_{23}-\hat{H}_{22}\hat{H}_{14}\ . \tag{A12}$$

If the product $RS>0$, we define the quantities θ, $\nu_\pm$, and $\mu_\pm$ as follows [where we use $\epsilon(x)=x/|x|$, and $\Delta_{14}=\hat{H}_{11}\hat{H}_{44}-\hat{H}_{14}^2$]:

$$\tan\theta=\epsilon(S)(4\hat{\Omega}_+^2-\hat{H}_{11}\hat{H}_{22}+\hat{H}_{23}\hat{H}_{14})/(RS)^{1/2}\ ,$$
$$\nu_\pm=\tfrac{1}{2}\ln[(\hat{H}_{23}\Delta_{14}-4\hat{\Omega}_\pm^2\hat{H}_{14})/(2\hat{\Omega}_\pm S)]\ ,$$
$$\mu_\pm=\tfrac{1}{2}\ln(R/S)-\nu_\pm\ . \tag{A13}$$

The coefficients C may then be written in terms of θ, ν_+, and $\mu_\pm$ as

$$C_{+a}=\cos\theta\cosh\nu_+,\quad C_{+a*}=\cos\theta\sinh\nu_+\ ,$$
$$C_{+b}=\sin\theta\cosh\mu_+,\quad C_{+b*}=\sin\theta\sinh\mu_+\ ,$$
$$C_{-a}=\sin\theta\cosh\nu_-,\quad C_{-a*}=\sin\theta\sinh\nu_-\ ,$$
$$C_{-b}=-\cos\theta\cosh\mu_-,\quad C_{-b*}=-\cos\theta\sinh\mu_-\ . \tag{A14}$$

The inequalities $|C_{\pm a}|\geq|C_{\pm a*}|$ and $|C_{\pm b}|\geq|C_{\pm b*}|$ are satisfied by these expressions. This may be interpreted as saying that the amplitudes $A_\pm$ contain more of $(a-a_f)$ than $(a-a_f)^*$ and more of $(b-ib_f)$ than $(b-ib_f)^*$.

If the product $RS<0$, then there are two distinct subcases: (1) If

$$|\hat{H}_{11}\hat{H}_{22}-\hat{H}_{23}\hat{H}_{14}-4\hat{\Omega}_+^2|>|\hat{H}_{11}\hat{H}_{22}+\hat{H}_{23}\hat{H}_{14}-4\hat{\Omega}_-^2|\ ,$$

we define the quantities ξ, $\nu_\pm$, and $\mu_\pm$ by the expressions

$$\tanh\xi=\epsilon(S)(4\hat{\Omega}_-^2-\hat{H}_{11}\hat{H}_{22}-\hat{H}_{23}\hat{H}_{14})/(-RS)^{1/2}\ ,$$
$$\nu_\pm=\tfrac{1}{2}\ln[(4\hat{\Omega}_\pm^2\hat{H}_{14}-\hat{H}_{23}\Delta_{14})/(\pm2\hat{\Omega}_\pm S)]\ ,$$
$$\mu_\pm=\tfrac{1}{2}\ln(-R/S)-\nu_\pm\ . \tag{A15}$$

The coefficients are given by

$$C_{+a}=-\sinh\xi\sinh\nu_+,\quad C_{+a*}=-\sinh\xi\cosh\nu_+\ ,$$
$$C_{+b}=\cosh\xi\cosh\mu_+,\quad C_{+b*}=\cosh\xi\sinh\mu_+\ ,$$
$$C_{-a}=\cosh\xi\cosh\nu_-,\quad C_{-a*}=\cosh\xi\sinh\nu_-\ ,$$
$$C_{-b}=\sinh\xi\sinh\mu_-,\quad C_{-b*}=\sinh\xi\cosh\mu_-\ . \tag{A16}$$

The inequalities $|C_{+a}|\leq|C_{+a*}|$, $|C_{+b}|\geq|C_{+b*}|$, $|C_{-a}|\geq|C_{-a*}|$, and $|C_{-b}|\leq|C_{-b*}|$ hold.

(2) If, however,

$$|\hat{H}_{11}\hat{H}_{22}-\hat{H}_{23}\hat{H}_{14}-4\hat{\Omega}_+^2|<|\hat{H}_{11}\hat{H}_{22}-\hat{H}_{23}\hat{H}_{14}-4\hat{\Omega}_-^2|\ ,$$

then we define the quantities ξ, $\nu_\pm$, and $\mu_\pm$ by the expressions

$$\tanh\xi=\epsilon(S)(4\hat{\Omega}_+^2-\hat{H}_{11}\hat{H}_{22}+\hat{H}_{23}\hat{H}_{14})/(-RS)^{1/2}\ ,$$
$$\nu_\pm=\tfrac{1}{2}\ln[(\hat{H}_{23}\Delta_{14}-4\hat{\Omega}_\pm^2\hat{H}_{14})/(\pm2\hat{\Omega}_\pm S)]\ ,$$
$$\mu_+=\tfrac{1}{2}\ln(-R/S)-\nu_\pm\ . \tag{A17}$$

In this case the coefficients may be written as

$$C_{+a}=\cosh\xi\cosh\nu_+,\quad C_{+a*}=\cosh\xi\sinh\nu_+\ ,$$
$$C_{+b}=\sinh\xi\sinh\mu_+,\quad C_{+b*}=\sinh\xi\cosh\mu_+\ ,$$
$$C_{-a}=-\sinh\xi\sinh\nu_-,\quad C_{-a*}=-\sinh\xi\cosh\nu_-\ ,$$
$$C_{-b}=\cosh\xi\cosh\mu_-,\quad C_{-b*}=\cosh\xi\sinh\mu_-\ . \tag{A18}$$

Here the inequalities $|C_{+a}|\geq|C_{+a*}|$, $|C_{+b}|\leq|C_{+b*}|$, $|C_{-a}|\leq|C_{-a*}|$, and $|C_{-b}|\geq|C_{-b*}|$ hold, which are just the opposite of the preceding subcase.

Spontaneous-forward-direction-emission spectrum

The forward (and backward) spontaneous emission for an electron whose trajectory is similar to that predicted by our model may be calculated as follows. We consider only free-space emission and we simplify the electron's motion in the interest of transparency. The amplitude for the emission of positive (negative) helicity radiation of frequency $\hat{\omega}$ in the direction $\eta\hat{e}_z$, where $\eta=\pm1$, is denoted by $A_\pm(\hat{\omega})$ and we have the relation

$$A_-(\hat{\omega})=(A_+(-\hat{\omega}))^* \ . \tag{A19}$$

The intensities of definite helicity (energy per unit dimensionless frequency $\hat{\omega}$ in solid angle $d\Omega$) are given by

$$\frac{d^2I_\pm}{d\hat{\omega}\,d\Omega}=2ck_w|A_\pm(\hat{\omega})|^2 \ . \tag{A20}$$

Following Jackson's Eq. (14.64) [7], we write

$$A_+(\hat{\omega})=i\hat{\omega}\left[\frac{e^2}{16\pi^2c}\right]^{1/2} \times\int_0^{\hat{T}}d\hat{t}\,[\beta_x(\hat{t})-i\eta\beta_y(\hat{t})]e^{i\hat{\omega}[\hat{t}-\eta\hat{z}(\hat{t})]} \ , \tag{A21}$$

where $\hat{T}$ denotes the time spent in the wiggler.

In order to evaluate $A_+(\hat{\omega})$ we assume that the transverse position as a function of time is given by the expression

$$\hat{x}(\hat{t})+i\hat{y}(\hat{t})=(\hat{\rho}_f+\delta e^{i(\hat{\Xi}\hat{t}+\chi)})e^{i\hat{z}(\hat{t})} \ , \tag{A22}$$

where $\hat{\rho}_f$ is the scaled radius at the fixed point, δ is real, χ is a phase, and $\hat{\Xi}$ is a frequency. For the axial velocity we use

$$\beta_z(\hat{t})=\beta+\epsilon\cos(\hat{\Omega}\hat{t}+\psi) \ , \tag{A23}$$

where β is the mean axial velocity, ϵ is the ripple amplitude whose frequency is $\hat{\Omega}$, and ψ is a phase. In most cases of interest the frequencies $\hat{\Xi}$ and $\hat{\Omega}$ will be equal, but we allow them to be distinct here. The axial position as a function of time is then

$$\hat{z}(\hat{t})=\hat{z}(0)+\beta\hat{t}+(\epsilon/\hat{\Omega})[\sin(\hat{\Omega}\hat{t}+\psi)-\sin\psi] \ . \tag{A24}$$

Using the identity

$$e^{i\alpha\hat{z}(\hat{t})}=e^{i\alpha[\hat{z}(0)+\beta\hat{t}-(\epsilon/\hat{\Omega})\sin\psi]} \times\sum_{m=-\infty}^{\infty}J_m(\alpha\epsilon/\hat{\Omega})e^{im[\hat{\Omega}\hat{t}+\psi]} \ , \tag{A25}$$

where J_m denotes a Bessel function and α a real number, we find

$$A_+(\hat{\omega})=\frac{\hat{\omega}^2}{\hat{\omega}+1}\left[\frac{e^2}{16\pi^2c}\right]^{1/2}e^{-i\eta(\hat{\omega}+1)[\hat{z}(0)-(\epsilon/\hat{\Omega})\sin\psi]} \times\sum_{m=-\infty}^{\infty}\left\{J_{-m}[\eta(\hat{\omega}+1)\epsilon/\hat{\Omega}]e^{im\psi}\left[\hat{\rho}_f e^{i\alpha_m\hat{T}}\left[\frac{\sin\alpha_m\hat{T}}{\alpha_m}\right]+\delta(1+\eta\hat{\Xi})e^{i(\gamma_m\hat{T}-\eta\chi)}\left[\frac{\sin\gamma_m\hat{T}}{\gamma_m}\right]\right]\right\} . \tag{A26}$$

In this expression we have used the following substitutions:

$$\alpha_m=(1-\eta\beta)(\hat{\omega}-\hat{\omega}_m)/2 \ , \tag{A27}$$

$$\gamma_m=(1-\eta\beta)(\hat{\omega}-\hat{\omega}'_m)/2 \ , \tag{A28}$$

where the peak frequencies $\hat{\omega}_m$ and $\hat{\omega}'_m$ are defined by

$$\hat{\omega}_m=(\eta\beta-m\hat{\Omega})/(1-\eta\beta) \ , \tag{A29}$$

$$\hat{\omega}'_m=[\eta(\beta+\hat{\Xi})-m\hat{\Omega}]/(1-\eta\beta) \ . \tag{A30}$$

We have also neglected terms which remain finite when $\hat{T}$, which is approximately $2\pi N/\beta$, where N is the number of periods, becomes large. In this limit, the amplitude $A_+(\hat{\omega})$ is well represented by a sum of peaks at $\hat{\omega}=\hat{\omega}_m$ and $\hat{\omega}=\hat{\omega}'_m$, whose relative sizes are determined mainly by the value of the Bessel function. The width of all peaks is approximately $\beta/[N(1-\eta\beta)]$, while the spacing between adjacent peaks in either series is $\hat{\Omega}/(1-\eta\beta)$. If the value of $\hat{\omega}_m$ or $\hat{\omega}'_m$ is negative, the radiation occurs at the positive frequency ($|\hat{\omega}_m|$ or $|\hat{\omega}_{m'}|$), but with *negative* helicity.

If the ripple ϵ and the quantity δ are set equal to zero, we recover

$$\lim_{\epsilon,\delta\to0}A_+(\hat{\omega})=\frac{\hat{\omega}^2}{\hat{\omega}+1}\left[\frac{e^2}{16\pi^2c}\right]^{1/2}e^{i[\alpha_0\hat{T}-\eta(\hat{\omega}+1)\hat{z}(0)]} \times\hat{\rho}_f\left[\frac{\sin\alpha_0\hat{T}}{\alpha_0}\right] , \tag{A31}$$

which corresponds to emission at the usual FEL frequency

$$\hat{\omega}_0=\eta\beta/(1-\eta\beta) \ , \tag{A32}$$

provided that $\eta\beta>0$. This condition simply means that the beam and radiation propagate in the same direction. If $\eta\beta<0$, then there is negative helicity radiation emitted in the direction opposite to the beam. However, its frequency is not increased by the Lorentz factor, and the intensity is necessarily small because of the explicit factor of $\hat{\omega}^4$. Henceforth we shall limit our attention to the case where $\eta\beta>0$.

If the velocity ripple ϵ is assumed to be small, but not zero, a reasonable approximation is to retain in Eq. (A26) only the $m=0$ and $m=\pm1$ contributions. For $m=0$, the relevant term is $\propto J_0(\epsilon/[\hat{\Omega}(1-\eta\beta)])$, which is ≈1, for very small ϵ, but which is ≈0 if $\epsilon/[\hat{\Omega}(1-\eta\beta)]=2.4$. We

thus see that emission at the FEL frequency $\hat{\omega}_0$ can be quenched unless $\epsilon < 2.4\hat{\Omega}(1-\eta\beta)$. For highly relativistic electrons or small $\hat{\Omega}$, this suppression might occur.

The $m=1$ contribution peaks at frequency $\hat{\omega}_1=(\eta\beta-\hat{\Omega})/(1-\eta\beta)$, and it is governed by $J_1(\epsilon(1-\hat{\Omega})/[\hat{\Omega}(1-\eta\beta)])$. Similarly, the $m=-1$ contribution occurs at frequency $\hat{\omega}_{-1}=(\eta\beta+\hat{\Omega})/(1-\eta\beta)$, and it is proportional to $J_1(\epsilon(1+\hat{\Omega})/[\hat{\Omega}(1-\eta\beta)])$. In the group-I mode of operation, the ripple frequency $\hat{\Omega}\approx\beta-\hat{\Omega}_0/\gamma$, whereas for group II one has $\hat{\Omega}\approx\hat{\Omega}_0/\gamma-\beta$. From this we deduce the following approximate results:

group I: $\beta>\hat{\Omega}_0/\gamma$, $\hat{\omega}_1\approx(\hat{\Omega}_0/\gamma)/(1-\beta)$, $\hat{\omega}_{-1}\approx(2\beta-\hat{\Omega}_0/\gamma)/(1-\beta)$,

group II: $0<\beta<\hat{\Omega}_0/\gamma$, $\hat{\omega}_1\approx(2\beta-\hat{\Omega}_0/\gamma)/(1-\beta)$, $\hat{\omega}_{-1}\approx(\hat{\Omega}_0/\gamma)/(1-\beta)$,

reversed field: $\beta<0$, $\hat{\omega}_1\approx(-\hat{\Omega}_0/\gamma)/(1+\beta)$, $\hat{\omega}_{-1}\approx(\hat{\Omega}_0/\gamma-2\beta)/(1+\beta)$.

In each case one of the satellite frequencies is approximately equal to the boosted cyclotron frequency $\hat{\Omega}_0/[\gamma(1-|\beta|)]$, but for the reversed field, the frequency $\hat{\omega}_1$ is negative, which implies that the helicity is *negative*. If the FEL is operated at "antiresonance," $\hat{\Omega}_0/\gamma=-\beta$, then $\hat{\omega}_1=-\hat{\omega}_0$, which means that the spontaneous emission peak at the frequency $\hat{\omega}_0$ contains both helicities. We also note that when the pseudocrossing takes place (Group II), the frequency $\hat{\omega}_1$ vanishes.

To complete our discussion of the spontaneous-emission spectrum, we consider the contribution proportional to δ in Eq. (A26). Since δ is supposed to be small, keeping only the $m=0$ term in the sum is presumably a good approximation. Typically the frequency $\hat{\Xi}$ satisfies the approximate relation $\beta+\hat{\Xi}=\hat{\Omega}_0/\gamma$, which implies that the spontaneous-emission frequency $\hat{\omega}_0'$ is given by

$$\hat{\omega}_0'\approx\begin{cases}(\hat{\Omega}_0/\gamma)/(1-\beta) & \text{(groups I and II)},\\ (-\hat{\Omega}_0/\gamma)/(1+\beta) & \text{(reversed field)}.\end{cases}$$

Thus the principal contribution of the δ term occurs at the boosted cyclotron frequency, just as did one of the satellite terms caused by the ripple frequency. For reversed-field operation the negative frequency implies *negative* helicity.

[1] H. P. Freund and A. K. Ganguly, IEEE J. Quantum Electron. **QE-21**, 1073 (1985).

[2] C. Chen and R. C. Davidson, Phys. Rev. A **43**, 5541 (1991).

[3] G. Spindler and G. Renz, Phys. Fluids B **3**, 3517 (1991).

[4] M. E. Conde and G. Bekefi, Phys. Rev. Lett. **67**, 3082 (1991).

[5] W. B. Colson and A. M. Sessler, Annu. Rev. Nucl. Part. Sci. **35**, 25 (1985).

[6] H. Bottolier-Curtet *et al.*, *Proceedings of the Twelfth International FEL Conference, Paris, France, 1990* [Nucl. Instrum. Methods A **304**, 311 (1991)].

[7] J. D. Jackson, *Classical Electrodynamics* (Wiley, New York, 1975).

[8] J. M. J. Madey, Nuovo Cimento B **50**, 34 (1979).

[9] K. R. Chu and A. T. Lin, Phys. Rev. Lett. **67**, 3235 (1991).

[10] E. T. Whittaker, *A Treatise on the Analytical Dynamics of Particles and Rigid Bodies* (Cambridge University Press, Cambridge, England, 1960), p. 413.

[11] J. L. Rullier, thèse, Université de Bordeaux I, 1992 (unpublished).

[12] J. P. Blewett and R. Chasman, J. Appl. Phys. **48**, 2692 (1977).

[13] H. Goldstein, *Classical Mechanics* (Addison-Wesley, Reading, MA, 1950).

[14] A similar set of canonical variables were used by Chen and Davidson in Ref. [2].

[15] E. T. Whittaker and G. Watson, *A Course of Modern Analysis* (Cambridge University Press, Cambridge, England, 1962).

[16] L. Friedland, Phys. Fluids **23**, 2376 (1980).